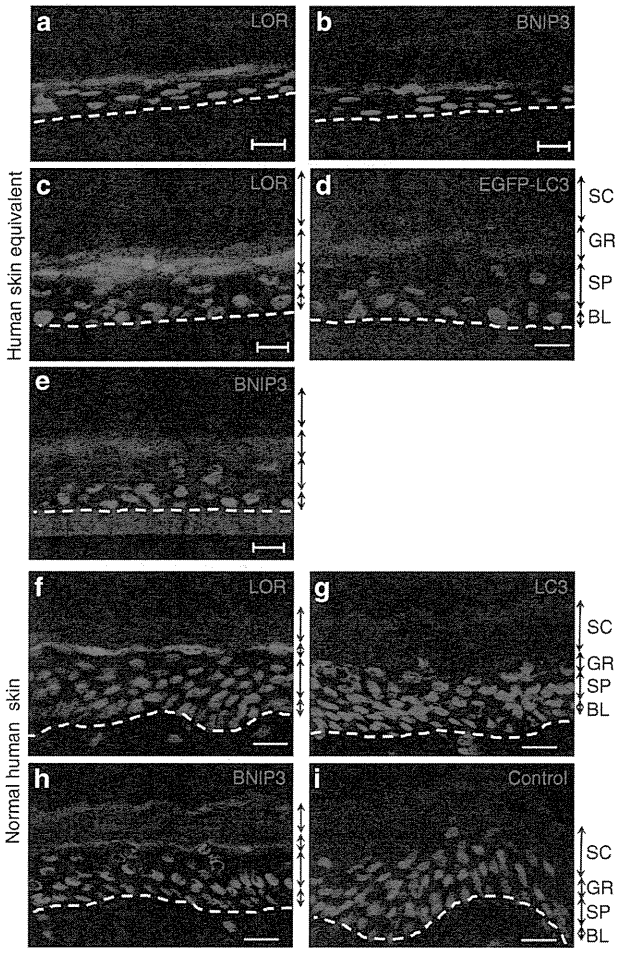

Figure 2. BNIP3 (BCL2 and adenovirus E1B 19-kDa-interacting protein 3) is expressed in the granular layer of the human epidermis. (**a–e**) Human skin epidermal equivalents were constituted from (**a–d**) normal human primary epidermal keratinocytes (HPEKs) or (**e**) HPEKs transfected with EGFP-LC3 by lentiviral vector. Cells were grown for (**a**, **b**) 18 days and (**c–e**) 24 days after exposure at the air–liquid interface. (**f–i**) Normal human skin epidermis. (**a**, **c**, **f**) Expression pattern of loricrin (LOR). (**b**, **e**, **h**) Expression pattern of BNIP3. (**i**) Control staining without BNIP3 antibody is shown. (**d**) Autophagosome formation determined by EGFP-LC3 puncta. (**g**) Endogenous expression pattern of LC3. The blue signals indicate nuclear staining. The dotted lines indicate (**a–e**) the boundary between the epidermis and the membrane or (**f–i**) the boundary between the epidermis and the dermis. Scale bars = 20 μm. BL, basal layer; GL, granular layer; SC, stratum corneum (cornified layer); SP, spinous layer.

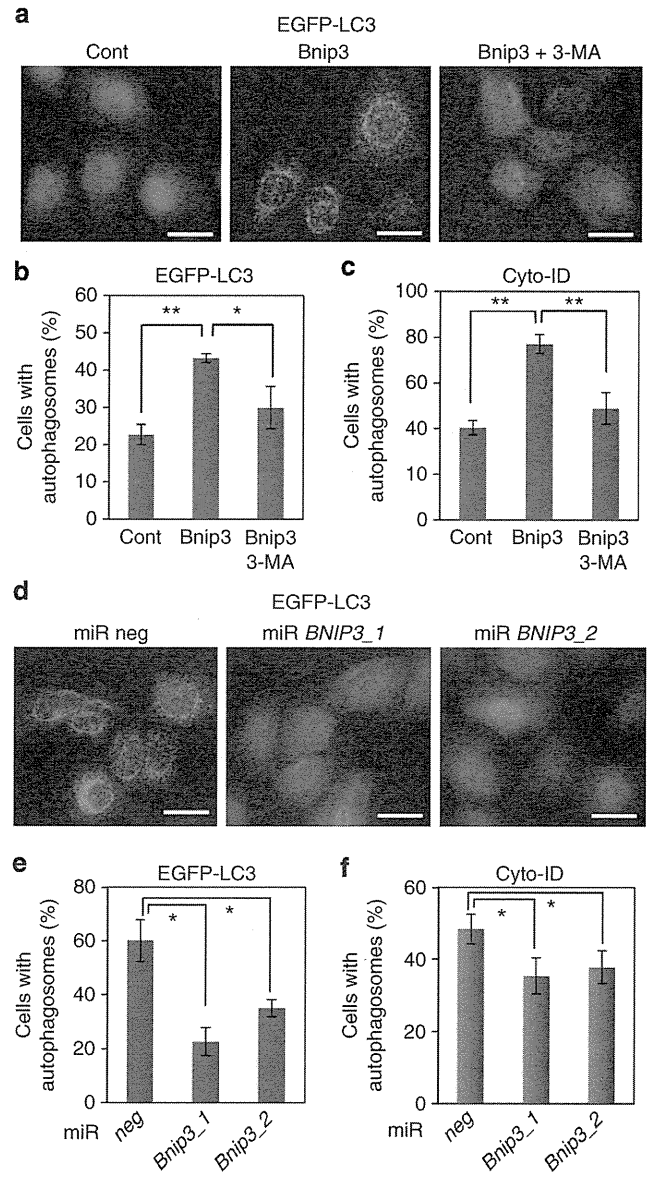

Figure 3. BNIP3 (BCL2 and adenovirus E1B 19-kDa-interacting protein 3) stimulates autophagy. (**a**, **b**) EGFP-LC3-expressing human primary epidermal keratinocytes (HPEKs) were transduced with DsRed (Cont) or BNIP3. As an inhibitor of autophagy, 3-methyladenine 3-MA (5 mM) was added. Cells were then stained with anti-EGFP at 24 hours after transduction. (**a**) EGFP-LC3 staining is shown in green. Scale bars = 20 μm. (**b**) The percentage of EGFP-LC3-positive cells with more than five puncta were quantified and are presented as the mean of three independent experiments ± SD. (**c**) HPEKs were transduced with DsRed (Cont) or BNIP3. As an inhibitor of autophagy, 3-MA (5 mM) was added. Autophagy induction was determined by Cyto-ID staining and quantified by flow cytometry. (**d**, **e**) EGFP-LC3-expressing HPEKs were transduced with miR *neg*, miR *BNIP3_1*, or miR *BNIP3_2* and induced to differentiate. Cells were then stained with anti-EGFP at 8 hours after differentiation induction. (**d**) EGFP-LC3 staining is shown in green. Scale bars = 20 μm. (**e**) The percentage of EGFP-LC3-positive cells with more than five puncta were quantified and are presented as the mean of three independent experiments ± SD. (**f**) HPEKs were transduced with miR *neg*, miR *BNIP3_1*, or miR *BNIP3_2* and induced to differentiate. Autophagy induction was determined by Cyto-ID staining and quantified by flow cytometry. All the data represent the average of three independent experiments ± SD. $^{**}P<0.01$; $^{*}0.01<P<0.05$.

that "sunburn-like cells" existed in BNIP3 knockdown epidermal equivalent (Figure 6a and b). We therefore hypothesized that BNIP3 might play a key role in the survival of epidermal keratinocytes. To evaluate this hypothesis, HPEKs were irradiated with 20 mJ cm^{-2} UVB. UVB irradiation triggered the formation of autophagosome that was significantly reduced by BNIP3 knockdown (Figure 6c–e). As shown in Figure 6f, UVB irradiation induced cleavage of caspase3 and BNIP3 expression. Intriguingly, knockdown of UVB-induced BNIP3 by RNAi further increased the amount of cleaved caspase3, suggesting that BNIP3 is required for the protection of keratinocytes from UVB-induced apoptosis (Figure 6f).

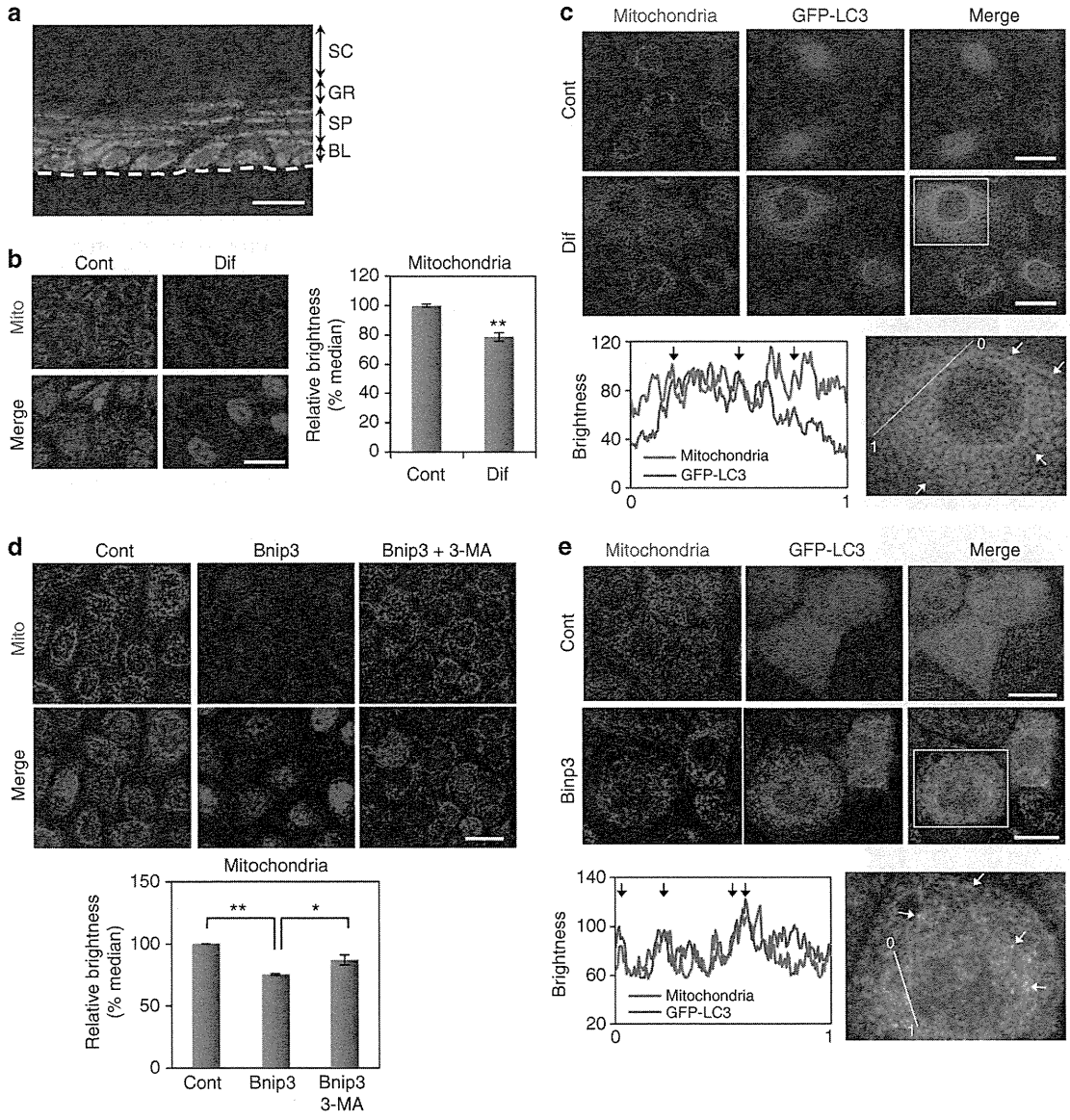

Figure 4. Autophagy stimulates mitochondrial degradation. (**a**) Distribution pattern of mitochondria. The blue signals indicate nuclear staining. The dotted lines indicate the boundary between the epidermis and the membrane. Scale bars = 20 μm. BL, basal layer; GL, granular layer; SC, stratum corneum (cornified layer); SP, spinous layer. (**b**) Nondifferentiated control (Cont) or differentiated human primary epidermal keratinocytes (HPEKs; Dif) were subjected to immunofluorescent staining 2 days after induction of differentiation. Mitochondrial staining is shown in red. The blue signals indicate nuclear staining. Scale bar = 20 μm. The graph indicates the percent of median brightness calculated by BZ Analyzer Software (Keyence) as the mean of three independent experiments ± SD. (**c**) EGFP-LC3-expressing HPEKs were differentiated. Cont or Dif were stained with anti-mitochondria (red) and anti-EGFP (green) 8 hours after induction of differentiation. Graph indicates the linescan analysis of the red and green fluorescent channels. Initial point of linescan is indicated as 0, and terminal point is indicated as 1. The arrows mark the colocalization of the two proteins. (**d**) HPEKs were transduced with enhanced green fluorescent protein (EGFP; Cont) or BNIP3 (BCL2 and adenovirus E1B 19-kDa-interacting protein 3). As an inhibitor of autophagy, 3-methyladenine 3-MA (5 mM) was added. Cells were then fixed and stained with anti-mitochondria 48 hours after transduction. Scale bar = 20 μm. The graph indicates the percent of median brightness calculated by BZ Analyzer Software (Keyence) as the mean of three independent experiments. $^{**}P<0.01$; $^{*}0.01<P<0.05$. (**e**) EGFP-LC3-expressing HPEKs were transduced with mock (Cont) or BNIP3. Cells were then fixed and stained with anti-mitochondria (red) and anti-EGFP (green) 24 hours after transduction. Graph indicates the linescan analysis of the red and green fluorescent channels. Initial point of linescan is indicated as 0, and terminal point is indicated as 1. The arrows mark the colocalization of the two proteins.

DISCUSSION

In this study, we demonstrated that BNIP3, a potent inducer of autophagy, plays a role in the terminal differentiation and maintenance of epidermal keratinocytes. It has been suggested that autophagy plays a role in the skin epidermis, but few attempts have been made to clarify the involvement of autophagy in skin epidermis.

We found that the HES1 transcriptional repressor directly suppressed BNIP3 expression in mouse epidermis and HPEKs (Figure 1). Moreover, our results revealed that BNIP3 was

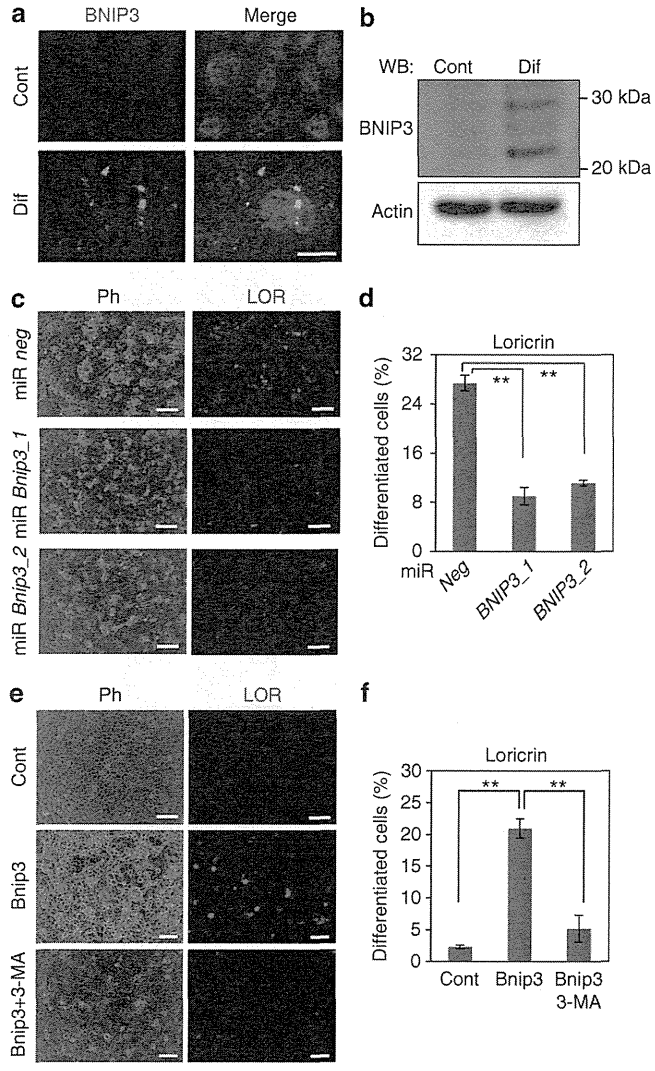

Figure 5. BNIP3 (BCL2 and adenovirus E1B 19-kDa-interacting protein 3) is required for the differentiation of keratinocytes *in vitro*. (**a**, **b**) Human primary epidermal keratinocytes (HPEKs) were differentiated and BNIP3 expression was observed. (**a**) Nondifferentiated control (Cont) or differentiated HPEKs (Dif) were subjected to immunofluorescent staining. BNIP3 staining is shown in green. Mitochondrial staining is shown in red. The blue signals indicate nuclear staining. Scale bar = 20 μm. (**b**) Western blot (WB) analysis. Proteins extracted from Cont or Dif were probed with anti-BNIP3 or anti-actin. (**c**, **d**) HPEKs were infected with adenoviral vectors expressing miR *neg*, miR *BNIP3_1*, or miR *BNIP3_2* followed by induction of differentiation. Cells were then immunostained with a loricrin antibody 9 days after transduction. (**e**, **f**) HPEKs were infected with adenoviral vectors expressing enhanced green fluorescent protein (EGFP; Cont) or BNIP3 and subjected to immunofluorescent staining against loricrin (LOR) 6 days after transduction. As an inhibitor of autophagy, 3-methyladenine 3-MA (5 mM) was added. Phase contrast images (Ph) and LOR staining are shown. Scale bars = 200 μm. (**d**, **f**) Percentages of LOR-positive differentiated cells were calculated by computerized image analysis. The data represent the average of three independent experiments ± SD. $^{**}P<0.01$.

expressed in the granular layers of mouse epidermis, its human skin epidermal equivalent, and its normal human skin epidermis (Figures 1 and 2). These data are consistent with our previous report showing that Hes1 is expressed in the spinous layers, where it represses the regulatory genes for differentiation to maintain the spinous cell fate (Moriyama *et al.*, 2008). Hence, it can be inferred that Bnip3 expression is suppressed in the spinous layers by Hes1, whereas it is upregulated in the granular layers where Hes1 expression is absent. In addition, our finding that BNIP3 is required for keratinocyte differentiation fits our idea that Hes1 represses certain regulatory genes to prevent the premature differentiation of spinous cells. Our *in vitro* data suggest that BNIP3 is involved in keratinocyte differentiation through autophagy (Figures 3–5). The mechanisms underlying the involvement of autophagy in keratinocyte differentiation remain elusive; however, considering that keratinocyte differentiation induced mitochondrial clearance and BNIP3 expression (Figure 4 and 5), BNIP3-induced autophagy may be responsible for the removal of mitochondria that may be required for the terminal differentiation of epidermal keratinocytes. During reticulocyte differentiation, programmed clearance of mitochondria induced by BNIP3L/Nix, a molecule closely related to BNIP3, has been reported to be a critical step (Schweers *et al.*, 2007). Therefore, keratinocytes likely possess the same differentiation mechanism that reticulocytes have, although further investigation will be required for elucidation.

In contrast to the results from differentiation in two-dimensional culture, we did not observe drastic differentiation defects in the BNIP3 knockdown human epidermal equivalent except for the existence of "sunburn-like cells" (Figure 6). This might be because of the incomplete suppression of BNIP3 in the BNIP3 knockdown keratinocytes, and/or might be because of the redundancy between BNIP3 and BNIP3L/Nix, a homolog of BNIP3, as we found in our preliminary study that Bnip3l is also expressed in the epidermis (data not shown). Although the phenotypes of BNIP3-null mice were published in 2007, these researchers found that BNIP3-null mice had no increase in mortality or apparent physical abnormalities (Diwan *et al.*, 2007). Generally, impairment of epidermal differentiation or skin barrier formation results in an obvious defect. Thus, BNIP3-null epidermis seems to exhibit subtle, if any, abnormalities. On the basis of these findings, the involvement of BNIP3 in epidermal differentiation must be investigated in the future. In-depth analysis of the BNIP3-null epidermis phenotype could help elucidate the role of BNIP3 in mouse epidermal differentiation.

Despite the lack of obvious differentiation defects in the human epidermal equivalent, our data showing that BNIP3 knockdown caused the appearance of "sunburn-like cells" is regarded as an example of apoptosis (Young, 1987), revealing a new role of BNIP3 in keratinocyte maintenance. Furthermore, requirement of BNIP3 for protection from UV-induced apoptosis was confirmed in two-dimensional keratinocyte cultures (Figure 6e). The underlying mechanism of this prosurvival function of BNIP3 in keratinocytes remains unclear; however, previous reports have demonstrated that hypoxia-induced autophagy through BNIP3 is critical for the prosurvival process (Bellot *et al.*, 2009). Recently, it has been reported that UVA induces autophagy to remove oxidized phospholipids and protein aggregates in epidermal keratino-

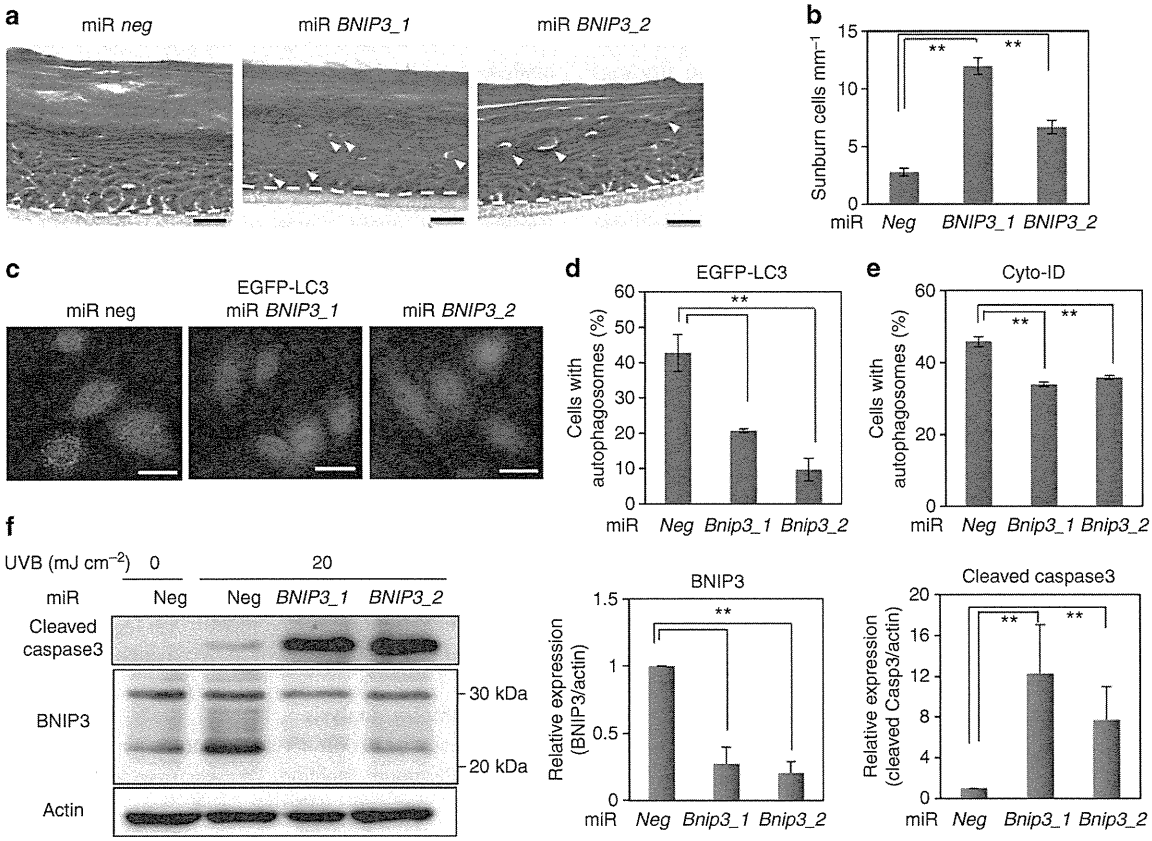

Figure 6. BNIP3 (BCL2 and adenovirus E1B 19-kDa-interacting protein 3) promotes cell survival in the reconstituted epidermis and keratinocytes. (**a**) Morphology of the human skin epidermal equivalents from human primary epidermal keratinocytes (HPEKs) infected with lentivirus expressing miR *neg*, miR *BNIP3_1*, or miR *BNIP3_2*. Arrowheads indicate sunburn-like cells. (**b**) The number of sunburn-like cells per mm was counted and plotted as the means of 10 sections ± SD. (**c–e**) HPEKs were infected with adenovirus expressing miR *neg*, miR *BNIP3_1*, or miR *BNIP3_2*, and irradiated with UVB. (**c**) Cells were stained with anti-EGFP at 8 hours after UVB irradiation. (**d**) The percentage of EGFP-LC3-positive cells with more than five puncta were quantified and are presented as the mean of three independent experiments ± SD. (**e**) Autophagy induction was determined by Cyto-ID staining and quantified by flow cytometry. The data represent the average of three independent experiments ± SD. (**f**) Cells were subjected to western blot analysis at 8 hours after irradiation. The blot shown is representative image of three independent experiments. Graphs indicate relative band intensities as determined by ImageJ software and plotted as the means of three independent experiments. Scale bars = 20 μm. $^{**}P<0.01$.

cytes (Zhao *et al.*, 2013). Because our data indicate that UVB-induced autophagy is mediated by BNIP3 (Figure 6c and d), it is possible that autophagy induced by BNIP3 also plays a role in the maintenance of keratinocytes. Further analysis is required to confirm these results.

UV-induced apoptotic cells appear within 12 hours and are predominately located in the suprabasal differentiated keratinocyte compartment of human skin (Gilchrest *et al.*, 1981). Moreover, differentiated keratinocytes appear to be most sensitive to the UV light that induces p53-dependent apoptosis (Tron *et al.*, 1998). Tron *et al.* (1998) demonstrated that differentiated keratinocytes in p53-null mice exhibited only a small increase in apoptosis after UVB irradiation compared with the increase observed in normal control animals (Tron *et al.*, 1998). Interestingly, because p53 has been reported to directly suppress BNIP3 expression (Feng *et al.*, 2011), BNIP3 might be abundantly upregulated in suprabasal cells in p53-null animals, resulting in the resistance to UVB-induced apoptosis. Indeed, our preliminary study showed that p53 knockdown enhanced UV-induced BNIP3 expression in HPEKs (data not shown). Therefore, BNIP3 expression in suprabasal cells appears to be important for the protection of differentiated keratinocytes from normal environmental stress such as weak UV exposure *in vivo*.

A recent report on a role for autophagy in epidermal barrier formation and function was identified in *atg7*-deficient mice (Rossiter *et al.*, 2013). The authors showed that autophagy was constitutively active in the suprabasal epidermal layers as we report in this study (Figure 2). However, in contradiction to our results, the authors concluded that autophagy was not essential for the barrier function of the skin. This may be because of the presence of an alternative Atg5/Atg7-independent autophagic pathway (Nishida *et al.*, 2009) in the epidermis. This Atg5/Atg7-independent pathway is also independent of LC3, but forms Rab9-positive double-membrane vesicles. Moreover, protein degradation via this pathway is inhibited by 3-MA and is dependent on Beclin 1. Our data demonstrate that: (1) BNIP3 induced the formation of

EGFP-LC3 puncta (Figure 4) and (2) 3-MA significantly diminished the formation of GFP-LC3 puncta and keratinocyte differentiation induced by BNIP3 (Figure 5). These findings suggest that BNIP3 in the epidermis induced both conventional and Atg5/Atg7-independent autophagy. Intriguingly, GFP cleaved from GFP-LC3 also accumulates in the *Atg7*-deficient epidermis (Rossiter *et al.*, 2013), thereby demonstrating the existence of an alternative autophagic pathway (Juenemann and Reits, 2012) in the epidermis. Further investigation will be required to determine whether Beclin 1 and Rab9 are indispensable for the BNIP3-induced autophagy and subsequent differentiation of keratinocytes.

In summary, our data reveal that expression of BNIP3 in granular cells induces autophagy and is involved in the terminal differentiation and maintenance of skin epidermis. Studies on the involvement of autophagy in skin epidermis have attracted considerable attention recently. In addition, increasing evidence suggests the involvement of BNIP3 in the differentiation of several cell types, including oligodendrocytes (Itoh *et al.*, 2003), osteoclasts (Knowles and Athanasou, 2008), and chondrocytes (Zhao *et al.*, 2012); however, the precise role of BNIP3 in this process remains to be investigated. Our study thus provides new insights into the functions of BNIP3 in differentiation and homeostasis.

MATERIALS AND METHODS

Histology and immunofluorescent analysis

Samples and embryos were fixed in 4% paraformaldehyde, embedded in optimal cutting temperature compound, frozen, and sectioned at 10 μm. Sections were then either subjected to hematoxylin and eosin staining or immunohistochemical analysis as previously described (Moriyama *et al.*, 2006). Details are described in Supplementary Materials Online.

Cell culture

HPEKs were purchased from CELLnTEC (Bern, Switzerland) and maintained in CnT-57 (CELLnTEC) culture medium according to the manufacturer's protocol. For induction of differentiation, the medium was changed to CnT-02 (CELLnTEC) at confluent monolayers of HPEKs, followed by adding calcium ions to 1.8 mM. The generation of human skin equivalents was performed using CnT-02-3DP culture medium (CELLnTEC) according to the manufacturer's protocol.

Design of artificial microRNAs and plasmid construction

Oligonucleotides targeting a human BNIP3 sequence compatible for use in cloning into BLOCK-iT Pol II miR RNAi expression vectors (Invitrogen, Carlsbad, CA) were obtained using the online tool BLOCK-iT RNAi Designer. The oligonucleotide sequences used in this study are shown in Supplementary Table S1 online. Cloning procedures were performed following the manufacturer's instructions.

Adenovirus and lentivirus infection

Adenoviruses expressing EGFP, Hes1, BNIP3, and miR *BNIP3* were constructed using the ViraPower adenoviral expression system (Invitrogen) according to the manufacturer's protocol. Lentivirus expressing EGFP-LC3 (from Addgene plasmid 21073, Cambridge, MA) and miR *BNIP3* plasmid was constructed and used to infect keratinocytes as previously described (Moriyama *et al.*, 2012; Moriyama *et al.*, 2013).

RNA extraction, complementary DNA generation, and Q-PCR

Total RNA extraction, complementary DNA generation, and Q-PCR analyses were carried out as previously described (Moriyama *et al.*, 2012). Details of the primers used in these experiments are shown in Supplementary Table S2 online.

Western blot analysis

Western blot analysis was performed as previously described (Moriyama *et al.*, 2012; Moriyama *et al.*, 2013). Details are described in Supplementary Materials Online.

ChIP assay

The ChIP assay was performed using the SimpleChIP Enzymatic Chromatin IP Kit (Magnetic Beads) (Cell Signaling Technology, Danvers, MA) according to the manufacturer's instructions. Hemagglutinin-tagged Hes1 was immunoprecipitated with rabbit polyclonal antibody against hemagglutinin tag (ab9110, Abcam, Cambridge, MA). Immunoprecipitated DNA was analyzed by Q-PCR. Relative quantification using a standard curve method was performed, and the occupancy level for a specific fragment was defined as the ratio of immunoprecipitated DNA over input DNA. Details of the primers used in these experiments are shown in Supplementary Table S2 online.

Flow cytometry analysis

For autophagy detection, Cyto-ID Autophagy detection kit (Enzo Life Sciences, Plymouth Meeting, PA) was used according to the manufacturer's instructions. Details are described in Supplementary Materials Online.

CONFLICT OF INTEREST

The authors state no conflict of interest.

ACKNOWLEDGMENTS

We thank Shogo Nomura, Ayumi Kitagawa, and Riho Ishihama for technical support; Dr Takashi Ueno for helpful discussions; Dr Hiroyuki Miyoshi for the CSII-EF-RfA, pCMV-VSVG-RSV-Rev, and pCAG-HIVg/p plasmids; Dr Tamotsu Yoshimori for pEGFP-LC3 plasmid; and Dr Ryoichiro Kageyama for *Hes1* KO mice. This work was supported by MEXT KAKENHI grant 23791304 to MM. This work was also supported in part by grants from the Ministry of Health, Labor, and Welfare of Japan and a grant from the Program for Promotion of Fundamental Studies in Health Sciences of the National Institute of Biomedical Innovation (NIBIO).

SUPPLEMENTARY MATERIAL

Supplementary material is linked to the online version of the paper at http://www.nature.com/jid

REFERENCES

Aymard E, Barruche V, Naves T *et al.* (2011) Autophagy in human keratinocytes: an early step of the differentiation? *Exp Dermatol* 20:263–8

Bellot G, Garcia-Medina R, Gounon P *et al.* (2009) Hypoxia-induced autophagy is mediated through hypoxia-inducible factor induction of BNIP3 and BNIP3L via their BH3 domains. *Mol Cell Biol* 29:2570–81

Blanpain C, Lowry WE, Pasolli HA *et al.* (2006) Canonical notch signaling functions as a commitment switch in the epidermal lineage. *Genes Dev* 20:3022–35

Chan LL, Shen D, Wilkinson AR *et al.* (2012) A novel image-based cytometry method for autophagy detection in living cells. *Autophagy* 8:1371–82

Chatterjea SM, Resing KA, Old W *et al.* (2011) Optimization of filaggrin expression and processing in cultured rat keratinocytes. *J Dermatol Sci* 61:51–9

Diwan A, Krenz M, Syed FM *et al.* (2007) Inhibition of ischemic cardiomyocyte apoptosis through targeted ablation of Bnip3 restrains postinfarction remodeling in mice. *J Clin Invest* 117:2825–33

Feng X, Liu X, Zhang W *et al.* (2011) p53 directly suppresses BNIP3 expression to protect against hypoxia-induced cell death. *EMBO J* 30: 3397–415

Gilchrest BA, Soter NA, Stoff JS *et al.* (1981) The human sunburn reaction: histologic and biochemical studies. *J Am Acad Dermatol* 5:411–22

Hamacher-Brady A, Brady NR, Logue SE *et al.* (2007) Response to myocardial ischemia/reperfusion injury involves Bnip3 and autophagy. *Cell Death Differ* 14:146–57

Haruna K, Suga Y, Muramatsu S *et al.* (2008) Differentiation-specific expression and localization of an autophagosomal marker protein (LC3) in human epidermal keratinocytes. *J Dermatol Sci* 52:213–5

Ishibashi M, Moriyoshi K, Sasai Y *et al.* (1994) Persistent expression of helix-loop-helix factor HES-1 prevents mammalian neural differentiation in the central nervous system. *EMBO J* 13:1799–805

Itoh T, Itoh A, Pleasure D (2003) Bcl-2-related protein family gene expression during oligodendroglial differentiation. *J Neurochem* 85:1500–12

Juenemann K, Reits EA (2012) Alternative macroautophagic pathways. *Int J Cell Biol* 2012:189794

Kabeya Y, Mizushima N, Ueno T *et al.* (2000) LC3, a mammalian homologue of yeast Apg8p, is localized in autophagosome membranes after processing. *EMBO J* 19:5720–8

Knowles HJ, Athanasou NA (2008) Hypoxia-inducible factor is expressed in giant cell tumour of bone and mediates paracrine effects of hypoxia on monocyte-osteoclast differentiation via induction of VEGF. *J Pathol* 215:56–66

Lippens S, Denecker G, Ovaere P *et al.* (2005) Death penalty for keratinocytes: apoptosis versus cornification. *Cell Death Differ* 12(Suppl 2):1497–508

Mellor HR, Rouschop KM, Wigfield SM *et al.* (2010) Synchronised phosphorylation of BNIP3, Bcl-2 and Bcl-xL in response to microtubule-active drugs is JNK-independent and requires a mitotic kinase. *Biochem Pharmacol* 79:1562–72

Mizushima N, Levine B (2010) Autophagy in mammalian development and differentiation. *Nat Cell Biol* 12:823–30

Mizushima N, Yamamoto A, Matsui M *et al.* (2004) In vivo analysis of autophagy in response to nutrient starvation using transgenic mice expressing a fluorescent autophagosome marker. *Mol Biol Cell* 15:1101–11

Mizushima N, Yoshimori T, Levine B (2010) Methods in mammalian autophagy research. *Cell* 140:313–26

Moriyama H, Moriyama M, Sawaragi K *et al.* (2013) Tightly regulated and homogeneous transgene expression in human adipose-derived mesenchymal stem cells by lentivirus with tet-off system. *PLoS One* 8:e66274

Moriyama M, Durham AD, Moriyama H *et al.* (2008) Multiple roles of Notch signaling in the regulation of epidermal development. *Dev Cell* 14:594–604

Moriyama M, Moriyama H, Ueda A *et al.* (2012) Human adipose tissue-derived multilineage progenitor cells exposed to oxidative stress induce neurite outgrowth in PC12 cells through p38 MAPK signaling. *BMC Cell Biol* 13:21

Moriyama M, Osawa M, Mak SS *et al.* (2006) Notch signaling via Hes1 transcription factor maintains survival of melanoblasts and melanocyte stem cells. *J Cell Biol* 173:333–9

Nishida Y, Arakawa S, Fujitani K *et al.* (2009) Discovery of Atg5/Atg7-independent alternative macroautophagy. *Nature* 461:654–8

Ohtsuka T, Ishibashi M, Gradwohl G *et al.* (1999) Hes1 and Hes5 as notch effectors in mammalian neuronal differentiation. *EMBO J* 18:2196–207

Quinsay MN, Thomas RL, Lee Y *et al.* (2010) Bnip3-mediated mitochondrial autophagy is independent of the mitochondrial permeability transition pore. *Autophagy* 6:855–62

Rossiter H, Konig U, Barresi C *et al.* (2013) Epidermal keratinocytes form a functional skin barrier in the absence of Atg7 dependent autophagy. *J Dermatol Science* 71:67–75

Sassone J, Colciago C, Marchi P *et al.* (2010) Mutant Huntingtin induces activation of the Bcl-2/adenovirus E1B 19-kDa interacting protein (BNip3). *Cell Death Dis* 1:e7

Schweers RL, Zhang J, Randall MS *et al.* (2007) NIX is required for programmed mitochondrial clearance during reticulocyte maturation. *Proc Natl Acad Sci USA* 104:19500–5

Sowter HM, Ratcliffe PJ, Watson P *et al.* (2001) HIF-1-dependent regulation of hypoxic induction of the cell death factors BNIP3 and NIX in human tumors. *Cancer Res* 61:6669–73

Srinivas V, Bohensky J, Shapiro IM (2009) Autophagy: a new phase in the maturation of growth plate chondrocytes is regulated by HIF, mTOR and AMP kinase. *Cells Tissues Organs* 189:88–92

Tron VA, Trotter MJ, Tang L *et al.* (1998) p53-regulated apoptosis is differentiation dependent in ultraviolet B-irradiated mouse keratinocytes. *Am J Pathol* 153:579–85

Vengellur A, LaPres JJ (2004) The role of hypoxia inducible factor 1alpha in cobalt chloride induced cell death in mouse embryonic fibroblasts. *Toxicol Sci* 82:638–46

Walls KC, Ghosh AP, Ballestas ME *et al.* (2009) bcl-2/Adenovirus E1B 19-kd interacting protein 3 (BNIP3) regulates hypoxia-induced neural precursor cell death. *J Neuropathol Exp Neurol* 68:1326–38

Young AR (1987) The sunburn cell. *Photodermatology* 4:127–34

Zhang J, Ney PA (2009) Role of BNIP3 and NIX in cell death, autophagy, and mitophagy. *Cell Death Differ* 16:939–46

Zhao Y, Chen G, Zhang W *et al.* (2012) Autophagy regulates hypoxia-induced osteoclastogenesis through the HIF-1alpha/BNIP3 signaling pathway. *J Cell Physiol* 227:639–48

Zhao Y, Zhang CF, Rossiter H *et al.* (2013) Autophagy is induced by UVA and promotes removal of oxidized phospholipids and protein aggregates in epidermal keratinocytes. *J Invest Dermatol* 133:1629–37

Journal of proteome research

Article

pubs.acs.org/jpr

Common Glycoproteins Expressing Polylactosamine-Type Glycans on Matched Patient Primary and Metastatic Melanoma Cells Show Different Glycan Profiles

Mitsuhiro Kinoshita,[†] Yosuke Mitsui,[†] Naotaka Kakoi,[†] Keita Yamada,[†] Takao Hayakawa,[‡] and Kazuaki Kakehi*[,†]

[†]School of Pharmacy, Kinki University, Kowakae 3-4-1, Higashi-Osaka 577-8502, Japan

[‡]Pharmaceutical Research and Technology Institute, Kinki University, Kowakae 3-4-1, Higashi-Osaka 577-8502, Japan

Supporting Information

ABSTRACT: Recently, we reported comparative analysis of glycoproteins which express cancer-specific *N*-glycans on various cancer cells and identified 24 glycoproteins having polylactosamine (polyLacNAc)-type *N*-glycans that are abundantly present in malignant cells [Mitsui et al., *J. Pharm. Biomed. Anal.* **2012**, *70*, 718−726]. In the present study, we applied the technique to comparative studies on common glycoproteins present in the matched patient primary and metastatic melanoma cell lines. Metastatic melanoma cells (WM266-4) contained a large amount of polyLacNAc-type *N*-glycans in comparison with primary melanoma cells (WM115). To identify the glycoproteins expressing these *N*-glycans, glycopeptides having polyLacNAc-type *N*-glycans were captured by a *Datura stramonium* agglutinin (DSA)-immobilized agarose column. The captured glycopeptides were analyzed by LC/MS after removing *N*-glycans, and some glycoproteins such as basigin, lysosome-associated membrane protein-1 (LAMP-1), and chondroitin sulfate proteoglycan 4 (CSPG4) were identified in both WM115 and WM266-4 cells. The expression level of polyLacNAc of CSPG4 in WM266-4 cells was significantly higher than that in WM115 cells. In addition, sulfation patterns of chondroitin sulfate (CS) chains in CSPG4 showed dramatic changes between these cell lines. These data show that characteristic glycans attached to common proteins observed in different stages of cancer cells will be useful markers for determining degree of malignancies of tumor cells.

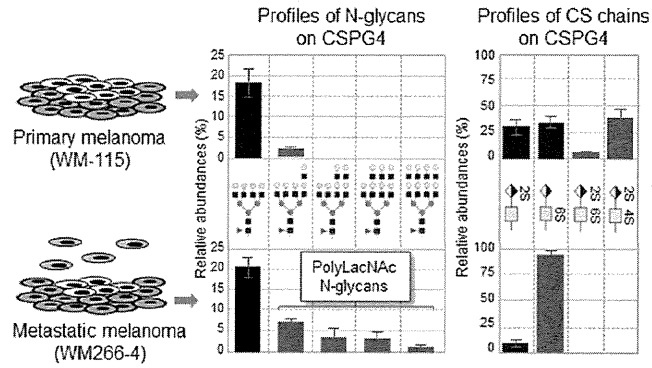

KEYWORDS: *polylactosamine, chondroitin sulfate, melanoma, malignant transformation*

INTRODUCTION

Glycosylation is one of the frequently observed post-translational modifications of proteins and plays various important roles such as protein folding, cellular communications, and signal transductions.[1,2] It is also well-known that embryonic development and cellular activation in mammalian cells are often accompanied by alterations in glycosylation. In addition, aberrant glycosylation has been known to be associated with various human diseases.[3−7] Expression of GlcNAc transferase V (GlcNAcT-V), which is the rate-limiting enzyme for the synthesis of polylactosamine (tandem repeating units of Galβ1-4GlcNAc at the nonreduing terminal ends), is increased in numerous cancer cells to cause increases of polyLacNAc-carrying *N*-glycans.[8−11] Colon cancer cells highly express sialyl-Lewis^x (NeuAcα2-3Galβ1-4[Fucα1-3] GlcNAc-R), while they show markedly decreased level of sialyl 6-sulfo Lewis^x compared with normal colonic cells.[12] Thus, alterations in glycosylation are a universal hallmark and prominent biomarkers for cancer.

Serological assays detect carbohydrate antigens such as sialyl-Le^x, sialyl-Le^a (CA19-9) and MUC16 (CA125). Sialyl-Le^x is a weak marker for some small-cell lung cancers (24% for all stages), however, sialyl-Le^x increases with tumor progression (71% for late-stage).[13] Unfortunately, elevation of these carbohydrate antigens is only suggestive of a cancer. α-Fetoprotein (AFP) is a well-known biomarker for liver diseases (e.g., cirrhosis, hepatitis, and hepatocellular carcinoma (HCC)), but its specificity for diagnosis of HCC is low (less than 50%). In contrast, fucosylated AFP (AFP-L3) is particularly useful in early detection of aggressive tumors associated with HCC with high specificity (>95%).[14] Alteration of serum α1-acid glycoprotein (AGP) has been reported to be associated with a risk of developing HCC during cirrhosis in chronic hepatitis. Kuno et al. statistically evaluated the relationship between the progression of liver fibrosis during cirrhosis and the decreased

Received: October 8, 2013
Published: December 19, 2013

α2−3 sialylation/the increased core α1-6fucosylation of *N*-glycans in AGP.[15]

Although time-consuming and laborious analysis is required for finding a candidate for cancer-specific biomarkers, detailed analysis of glycans in glycoconjugates provides us useful information for the development of novel biomarkers. In our previous reports, we proposed a series of methods for the analysis of glycans of glycoproteins in cancer cells.[16,17] Total glycan pool obtained from the cells was fluorescently labeled with 2-aminobenzoic acid (2-AA) and separated based on the number of sialic acid residues attached to the glycans using affinity chromatography on a serotonin-immobilized stationary phase. Total amounts of glycans as well as those of each category of glycans (asialo/high-mannose, mono-, di-, tri-, and tetra-sialoglycans) were determined based on their fluorescent intensities. This is very important information for determination of the expressed level of each category of the glycans. Then, the collected glycan groups were extensively analyzed by MS^n technique. On the basis of the studies using these techniques, we found that histiocytic lymphoma cells (U937), kidney glandular cells (ACHN), gastric cancer cells (MKN45), and lung cancer cells (A549) express a large amount of *N*-glycans having polyLacNAc residues.[16,17] To confirm glycoproteins which express these characteristic polyLacNAc-type *N*-glycans in cancer cells, tryptic-digested glycopeptides carrying multiple LacNAc units were captured using a *Datura stramonium* agglutinin (DSA)-immobilized column. The positions of peptides and glycans of the captured glycopeptides were analyzed by LC/MS^n-based technique after digestion with *N*-glycoamidase F, and we found that some glycoproteins such as CD107a and CD107b commonly contained polyLacNAc-type *N*-glycans in all the examined cancer cells. But integrin-α5 (CD49e) and carcinoembryonic antigen-related cell adhesion molecule 5 (CD66e) having these glycans were specifically found in U937 and MKN45 cells, respectively. These data indicate that specific glycans attached to specific proteins will be promising markers for specific tumors with high accuracy.[18]

Melanoma consists of an invasive tumors that are resistant to conventional therapy.[19] Therefore, monitoring of high-risk patients at early stage is highly recommended, but biomarkers for melanoma identification, prediction of progression, and prognosis are lacking. Although measurement of serum lactate dehydrogenase (LDH) is used for staging of melanoma, it is not specific for melanoma and cannot be used to predict progression or prognosis.[19] Melanoma inhibitory activity (MIA), a 11 kDa soluble protein, is present in the supernatant of the human melanoma cell line (HTZ-19). However, increased MIA levels are also observed in a subset of the patients with ovarian, pancreatic, breast, and colon cancer.[20] 5-*S*-Cysteinyldopa (5-S-CD) is produced in melanocytes and melanoma cells and has been reported to be raised particularly in late-stage (stage III and IV).[20] Thus, these biomarkers are detected frequently in the advanced stages of melanomas but are not useful for monitoring of stages or early detection of melanoma progression.

In the present study, we performed comparative studies on common glycoproteins present in the matched patient primary and metastatic melanoma cell lines, WM115 and WM266-4. At the initial step, total *N*-glycans expressed in both melanoma cells were comprehensively analyzed. Subsequently, glycoproteins having characteristic *N*-glycans that were observed in both cell lines were identified by combination of lectin-affinity capturing and bottom-up proteomics approaches. Among identified glycoproteins, chondroitin sulfate proteoglycan 4 (CSPG4) having both *N*-glycans and glycosaminoglycans (GAGs) was confirmed as a convincing marker for the melanoma-specific glycoproteins, and the structures of *N*-glycans and glycosaminoglycans of CSPG4 from each cell line were studied in deatil.

MATERIALS AND METHODS

Materials

Peptide *N*-glycoamidase F (EC 3.5.1.52) was obtained from Roche Diagnostics (Mannheim, Germany). Neuraminidase (*Arthrobacter ureafaciens*) was kindly donated by Dr. Ohta (Marukin-Bio, Uji, Kyoto, Japan). Benzonase was obtained from Novagen (Darmstadt, Germany). TPCK-treated trypsin was from Worthington (Lakewood, NJ). Anti-LAMP-1 (H4B3) mouse IgG1 monoclonal, and anti-CSPG4 (LHM2) mouse IgG monoclonal were from Santa Cruz Biotechnology (Santa Cruz, CA). Anti-Basigin (MEM-M6/1) mouse IgG1 monoclonal was from Abcam (Cambridge, U.K.). Iodoacetamide was from Tokyo Kasei Kogyo (Chuo-ku, Tokyo, Japan). Dithiothreitol (DTT) was obtained from Nacalai Tesque (Nakagyo-ku, Kyoto, Japan). 3,3′-Diaminobenzidine tetrahydrochloride (DAB) was obtained from DOJINDO (Kamimashiki-gun, Kumamoto, Japan). 2-Aminobenzoic acid (2-AA) and sodium cyanoborohydride for fluorescent labeling of oligosaccharides were from Tokyo Kasei. Coomassie brilliant blue G-250 was purchased from BIO-RAD (Hercules, CA). Sephadex LH-20 was from Amerscham Bioscience (Upsala, Sweden). Vivaspin 500 was obtained from Sartorius (Goettingen, Germany). *Datura stramonium* agglutinin (DSA)-agarose, chondroitinase ABC, and standard samples of unsaturated disaccharides derived from glycosaminoglycans were obtained from Seikagaku Kogyo (Chuoku, Tokyo, Japan). VECTA Elite ABC mouse IgG kit for Western blotting was obtained from Vector Laboratories (Burlingame, CA). Immobilon-P transfer membrane (PVDF) was from Millipore (Bedford, MA). Protein inhibitor cocktail for animal cells was obtained from Nacalai Tesque. Protein G Sepharose 4 Fast Flow was obtained from GE Healthcare (Upsala, Sweden). All other reagents and solvents were of the highest grade commercially available or of HPLC grade. All aqueous solutions were prepared using water purified with a Milli-Q purification system (Millipore, Bedford, MA).

Cell Culture

WM266-4 (human metastatic melanoma cells) and WM115 cells (human primary melanoma cells) derived from a same patient were employed as the materials. Both cells were cultured at 37 °C under 5% CO_2 atm in EMEM medium supplemented with 10% (v/v) fetal bovine serum, 2 mM glutamine, 1% nonessential amino acids (NEAA), and 1% sodium pyruvate. The cells were harvested at 80% confluent state, washed with phosphate buffered saline (PBS), and collected by centrifugation at 1000 rpm for 20 min.

Whole Proteins from Melanoma Cell Lines

Melanoma cells (1.0×10^7 cells) were suspended in PBS (50 μL) containing 1 mM EDTA and kept at room temperature for 15 min. Extraction reagent (7 M urea, 2 M thiourea, 4% CHAPS, 30 mM Tris-HCl (pH 8.5, 268 μL)), 1 M DTT (17 μL), and benzonase (125 units, 5 μL) were added to the suspended cells and kept at 37 °C for 30 min. The mixture was centrifuged at 8000*g* for 15 min. After addition of acetone

solution (85% acetone, 5% triethylamine, 5% acetic acid in water (1.7 mL)), the mixture was kept at −20 °C for 30 min and the precipitate was collected by centrifugation at 8000*g* for 15 min and washed with 75% ethanol (1 mL × 2). The precipitate was dried by a centrifugal evaporator.

Release of *N*-Glycans from Glycoproteins and Fluorescent Labeling of the Released *N*-Glycans with 2-Aminobenzoic acid (2-AA)

The whole protein pool obtained as described above was suspended in water (210 μL), 10% SDS (24 μL), and 2-mercaptoethanol (2.4 μL). The mixture was kept in the boiling water bath for 10 min. After cooling, 10% NP-40 solution (24 μL) and 1 M phosphate buffer (pH 7.5, 29 μL) were added. *N*-Glycoamidase F (4 U/4 μL) was added to the mixture and incubated at 37 °C for 24 h. After keeping the mixture in the boiling water bath for 5 min, the mixture was mixed with 695 μL of EtOH and centrifuged at 12000*g* for 15 min. The supernatant containing the released *N*-glycans was collected followed by lyophilization to dryness by a centrifugal evaporator. The dried mixture was dissolved in 2-AA (200 μL) solution prepared by dissolution of 2-AA (30 mg) and sodium cyanoborohydride (30 mg) in methanol (1 mL) containing 4% sodium acetate and 2% boric acid. The mixture was kept at 80 °C for 60 min. After addition of distilled water (200 μL), the mixture was applied to a column of Sephadex LH-20 (1.0 cm i.d., 30 cm length) equilibrated with 50% aqueous MeOH. The earlier eluted fluorescent fractions were collected and evaporated to dryness. The dried residue was dissolved in distilled water and used for the analysis of *N*-glycans.

Group Separation of 2-AA-Labeled *N*-Glycans Based on the Number of Sialic Acid Residues by Serotonin-Affinity Chromatography

Serotonin-affinity chromatography was performed by a Jasco HPLC apparatus equipped with two PU980 pumps and a Jasco FP920 fluorescence detector (Hachio-ji, Tokyo, Japan). An aqueous solution of the mixture of 2-AA-labeled *N*-glycans (10 μL, corresponded to 2.0 × 10^6 cells) was separated based on the number of sialic acid residues using a serotonin-immobilized column (4.6 mm i.d. × 150 mm length, J-Oilmils, Chu-o ku, Tokyo, Japan) by linear gradient from water (eluent A) to 40 mM ammonium acetate (eluent B) at a flow rate of 0.5 mL/min. Initially, eluent B was used at 5% concentration for 2 min, and then linear gradient elution was performed to 75% eluent B for 35 min, and finally the eluent was changed to 100% eluent B during the following 10 min. Peaks were collected and lyophilized to dryness.

NP-HPLC Analysis of 2-AA-Labeled *N*-glycans

Each group of *N*-glycans obtained by serotonin-affinity chromatography was further separated by normal-phase high-performance liquid chromatography after removing sialic acids by digestion with neuraminidase. A portion (10 μL, corresponded to 5 × 10^5 cells) of asialoglycans was analyzed with an Amide-80 column (Tosoh, 4.6 mm × 250 mm) using a linear gradient formed by 0.2% acetic acid in acetonitrile (solvent A) and 0.5% acetic acid in water containing 0.3% triethylamine (solvent B). The column was initially equilibrated and eluted with 30% solvent B for 2 min, from which point solvent B was increased to 95% over 80 min and kept at this composition for further 100 min. Flow rate was kept at 1.0 mL/min. The observed peaks were collected and lyophilized to dryness for the analysis by matrix-assisted laser-desorption ionization time-of-flight (MALDI-TOF) mass spectrometry (MS) according to the previous papers.[17,18] All *m*/*z* values of *N*-glycans were investigated using "Glyco-Peakfinder", which is a tool for annotation of glycan on MS-spectra (EuroCarbDB).

Lectin Affinity Chromatography of Glycopeptides Using a DSA-Immobilized Agarose Column

The whole protein pool from melanoma cells (1.0 × 10^7 cells) was dissolved in guanidine solution (2 mM EDTA, 0.5 M Tris-HCl, and 4 M guanidine (pH 8.5, 80 μL)), and 0.18 M DTT in guanidine solution (40 μL) was added to the mixture. The mixture was kept at 37 °C for 90 min. After addition of 0.18 M iodoacetamide in guanidine solution (55 μL), the mixture was kept for 45 min in a dark place. After addition of acetone solution (85% acetone, 5% triethylamine, 5% acetic acid in water (1.7 mL)), the mixture was kept at −20 °C for 30 min. The precipitate was collected by centrifugation at 8000*g* for 15 min and washed with 75% ethanol (1 mL × 2) and dried by a centrifugal evaporator. The dried material was digested with TPCK-treated trypsin (100 μg) in 0.1 M Tris-HCl (pH 8.6, 800 μL) containing 2 M urea at 37 °C overnight. After keeping the mixture at 100 °C for 10 min, the supernatant was collected and passed through an ultrafiltration membrane (MW cut off, 5000 Da). The residual solution on the membrane was used as a mixture of glycopeptides and applied to a DSA-immobilized column (DSA 3.8 mg (7.9 nmol)/1 mL of agarose), which had been previously equilibrated with PBS. Unbound peptides were eluted with PBS (15 mL). Then the bound glycopeptides were eluted with 0.1 M *N*-acetyl D-glucosamine in PBS (15 mL). The bound and unbound fractions were passed through an ultrafiltration membrane (MWCO, 3000 Da), respectively. The residual solutions on the membrane were evaporated to dryness by a centrifugal evaporator. DSA-bounded/unbound glycopeptides were suspended in a mixture of water (210 μL), 10% SDS (24 μL), and 2-mercaptoethanol (2.4 μL) and was kept in the boiling water bath for 10 min. After cooling, 10% NP-40 solution (24 μL) and 1 M phosphate buffer (pH 7.5, 29 μL) were added. *N*-Glycoamidase F (4 U/4 μL) was added to the mixtures and kept at 37 °C for 24 h. After keeping the mixtures in the boiling water bath for 5 min followed by centrifugation at 8000*g* for 10 min, the supernatant solutions were collected. One half of the solutions were used for the analysis of de-*N*-glycosylated peptides, and another half were used for the analysis of *N*-glycans after fluorescent labeling with 2-AA in the same manner as describe above.

Liquid Chromatography (LC)-Ion-Trap Time-of-Flight (IT-TOF) MS Analysis of Peptides

Positive electrospray ionization (ESI)-MS analyses were conducted with an LC-IT-TOF MS instrument (Shimadzu, Kyoto) connected with an HPLC system (two LC-20AD pumps, a CTO-20AC column oven, and a CBM-20A system controller; Shimadzu, Kyoto). A portion (3 μL, equivalent to 5 × 10^6 cells) of the aqueous solution of the peptide mixture obtained by digestion with *N*-glycoamidase F was injected to a reverse-phase column (HiQ sil C18 column, 2.1 mm × 150 mm; KYA TECH) and analyzed using the following gradient program. Solvent A was 5% acetonitrile/0.1% formic acid. Solvent B was 95% acetonitrile/0.1% formic acid. The column was initially equilibrated and eluted with 5% solvent B for 5 min, from which point solvent B was increased to 75% over 30 min at a flow rate of 0.2 mL/min. Column temperature was kept at 40 °C. The MS apparatus was operated at a probe voltage of 4.50 kV, CDL temperature of 200 °C, nebulizer gas

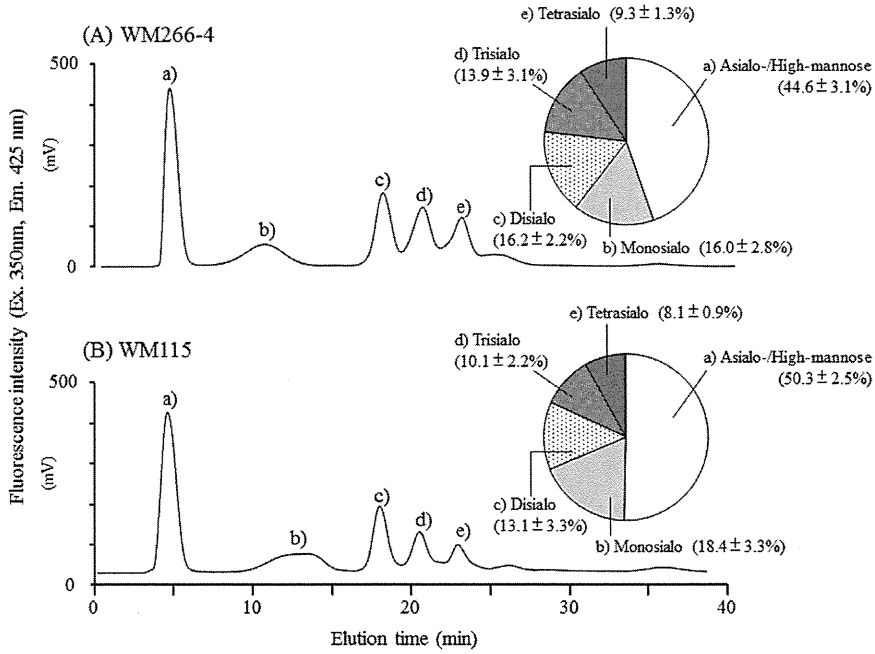

Figure 1. Serotonin-affinity chromatography of *N*-glycans derived from WM266-4 (A) and WM115 (B) cells. Analytical conditions: column, a serotonin-immobilized column (4.6 mm i.d., 150 mm length); eluent A, distilled water; eluent B, 40 mM ammonium acetate; gradient condition, linear gradient from 5% of eluent B to 75% of eluent B (2–37 min), and 75% of eluent B to 100% of eluent B for 10 min; flow rate, 0.5 mL/min; column temperature, 30 °C. Peak (a) asialo-/high mannose-type glycans, peak (b) monosialo-glycans, peak (c) disialo-glycans, peak (d) trisialo-glycans, peak (e) tetrasialo-glycan. The data in pie graphs were obtained by three experimental data.

flow of 1.5 L/min, and ion accumulation time of 30 ms. MS range was from m/z 200 to 2000, and MS/MS range also from m/z 200 to 2000. CID parameters were as follows: energy, 50%; collision gas, 50%. Monoisotopic ion was used as the precursor ion. MS data were processed with LCMS solution software ver. 3.6 (Shimadzu).

Peptide Mass Finger Printing

MS/MS spectra were processed using LCMS solution software version 3.6 (Shimadzu), and peak list files (Mascot generic format) for MS/MS ion search were generated using Mascot Distiller (version 2.3, Matrix Science). The parameters for database search were as follows. Protein database was set to Swiss PROT (version, 2011_12 containing 20323 human protein sequences). Taxonomy was set to *Homo sapiens*. One trypsin missed cleavage was allowed. The mass tolerance was set to 0.5 Da for precursor ions and 0.5 Da for product ions. Carbamidomethyl (C) was chosen as a fixed modification. Deamidated (NQ) was chosen for de-*N*-glycosylation (Asn (N) to Asp (D)). Peptide charge was chosen as +1, +2, and +3. Data format was chosen as Mascot generic, and instrument was chosen as ESI-TRAP-TOF. A decoy search (based on automatically generated random sequences) was employed to determine the false discovery rate (FDR) in MS/MS-based identification. The FDR was an average of 2.12% for all experiments.

Sodium Dodecyl Sulfate-Polyacrylamide Gel Electrophoresis (SDS-PAGE)

After addition of SDS-PAGE sample buffer (250 mM Tris-HCl (pH 6.8)-4.6% SDS, 20% glycerol), 2-mercaptoethanol, and water (10:9:1, 2 μL) to the whole protein (1×10^7 cells), the mixture was vortexed and boiled for 10 min. The supernatant was collected after centrifugation and used for SDS-PAGE. SDS-PAGE was performed with a Mini protean 3 cell and a POWER PAC 3000 (Bio Rad, Hercules, CA). The applied protein was 25 μg/lane as examined by the BCA method using bovine serum albumin as standard. Separation gel was 10%. Electrophoresis buffer was 25 mM Tris, 198 mM glycine, and 1% (w/v) SDS in water. After SDS-PAGE, the gel was stained with Coomassie brilliant blue G-250 (CBB) for 1 h. CBB solution contains 40% methanol, 10% acetic acid, and 0.2% CBB. The gel was destained with 40% methanol–10% acetic acid.

Western Blot Analysis

Western blot analysis was performed with a semidry electrophoretic transfer cell (Trans-Blot SD, BIO-RAD, Hercules, CA). PVDF membrane was previously kept in methanol for 1 min and in the blotting buffer (48 mM Tris, 39 mM glycine, and 20% methanol (pH9.0)) for 1 h. Each sample solution obtained as described above (25 μg as protein) from WM266-4 and WM115 cells was resolved using reducing 10% SDS-PAGE, and transferred to a PVDF membrane. The membrane was incubated in blocking buffer (5% skim milk, 0.05% Tween 20 in PBS). After washing the membrane with 0.05% Tween 20/PBS (20 mL × 4), the membrane was reacted with a primary antibody overnight. All the primary antibodies were used at the same concentration (5 μg/mL, 5 mL). After washing the membrane with 0.05% Tween 20/PBS (20 mL × 4), the membrane was reacted with the biotin conjugated secondary antibodies (5 μg/mL, 5 mL) for 1 h. After washing with 0.05% Tween 20/PBS (20 mL), the PVDF membrane was reacted with HRP labeled avidin (5 μg/mL, 5 mL in PBS) for 1 h. After washing with 0.05% Tween 20/PBS (20 mL × 4), the membrane was visualized with 0.05% DAB, 0.0031% hydrogen peroxide in 100 mM Tris-HCl buffer (pH 7.5).

Immunoprecipitation of Chondroitin Sulfate Proteoglycans 4 (CSPG4)

Anti-CSPG4 (50 μg/mL, 100 μL) was added to Protein G Sepharose (100 μL), and the mixture was incubated for 1 h.

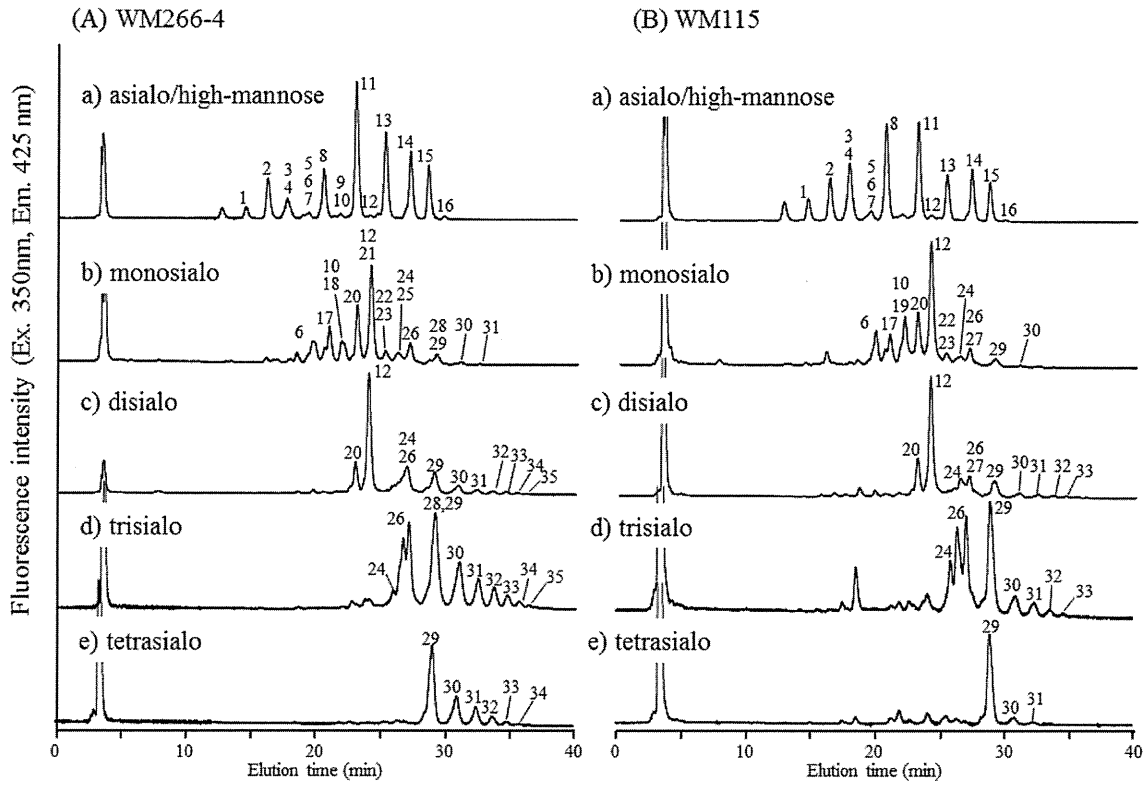

Figure 2. NP-HPLC analysis of five *N*-glycan fractions separated by serotonin-affinity chromatography. The *N*-glycans were previously digested with neuraminidase. Analytical conditions: column, TSK-Gel Amide-80 (4.6 mm × 250 mm); eluent A, 0.2% acetic acid/acetonitrile; eluent B, 0.5% acetic acid–0.3% triethylamine/water. Gradient elution, 0–2 min (30% solvent B), 2–82 min (30–95% solvent B), 82–102 min (95% solvent B). Detection, ex 350 nm, em 425 nm. Column temperature, 40 °C. The numbers on the peaks are those in the list of *N*-glycans of Table 1

Protein G Sepharose thus prepared was washed with PBS (1 mL × 3), and the protein mixture obtained from the cells (1 × 10^7 cells, see above) was added. The mixture was incubated at 4 °C overnight with gentle swirling. Protein G Sepharose was washed with PBS (1 mL × 6). After addition of SDS sample buffer (20 μL) and 2-mercaptoethanol (2 μL), Protein G Sepharose was boiled for 10 min. One half of the supernatant was collected by centrifugation and used for SDS-PAGE analysis, and the other half was used for the analysis of unsaturated disaccharides using capillary electrophoresis.

In-Gel Digestion with *N*-Glycoamidase F

Protein fractions collected by immunoprecipitation were analyzed by SDS-PAGE followed by staining with CBB. After changing the destaining solution with water, the positions detected by Western blot were cut, and the gel pieces were kept in 30% acetonitrile (300 μL × 2) for 30 min and dehydrated with acetonitrile (200 μL × 2) for 10 min.[18] After drying, the gel pieces were digested with *N*-glycoamidase F (2 U/2 μL) in 100 mM phosphate buffer (pH 7.5, 100 μL) at 37 °C overnight as described previously.[21] *N*-Glycans thus released were extracted with water (200 μL × 3) for 30 min, and the supernatant solution was used for labeling with 2-AA after evaporation to dryness.

Analysis of Unsaturated Disaccharides in CSPG4 Species Prepared by Immunoprecipitation from WM266-4 and WM115 Cells

A half of the fraction containing CSPG4 obtained by immunoprecipitation (see above) was dissolved in 50 mM Tris-HCl buffer (pH 8.0, 100 μL). Chondroitinase ABC (0.5 U) dissolved in the same buffer (10 μL) was added to the solution, and the mixture was kept at 37 °C for 12 h. The mixture of the unsaturated disaccharides thus eliminated was labeled with 2-AA according to the previously reported method[22] and analyzed by CE with a P/ACE MDQ Glycoprotein system (Beckman Coulter, Fullerton, CA, USA) equipped with a helium–cadmium laser-induced fluorescence detector (excitation 325 nm, emission 405 nm) using a fused silica capillary (50 μm i.d., 30 cm) in 0.1 M Tris-phosphate buffer (pH 3.0). Sample solutions were introduced into the capillary by pressure injection at 1 psi for 5 s and analyzed by applying voltage of −25 kV at 25 °C. Peaks observed on the electropherograms were assigned by coinjection with a mixture of standard unsaturated disaccharides (ΔdiCS-0S, ΔdiHA-0S, ΔdiCS-4S, ΔdiCS-6S, ΔdiCS-di2,6S ΔdiCS-di2,4S, ΔdiCS-di4,6S, and ΔdiCS-tri2,4,6S).

RESULTS AND DISCUSSION

Comparative Analysis of *N*-Glycans Expressed on WM266-4 and WM115 Cells

Total *N*-glycans prepared from WM266-4 and WM115 cells were separated based on the number of sialic acid residues using a serotonin-immobilized column as reported previously.[16,17] As shown in Figure 1, asialo-/high mannose-type *N*-glycans (peaks a) were not retained on the column and observed at ca. 5 min.

Monosialo- (peak b), disialo- (peak c), trisialo- (peak d), and tetrasialo- (peak e) *N*-glycans were observed at ca. 10–15 min, 18 min, 20 min, and 23 min, respectively. Asialo and high-mannose fractions were most abundant in both WM266-4 (44.6 ± 3.1%) and WM115 (50.3 ± 2.5%) cells. Relative abundances (18.4 ± 3.3%) of monosialo *N*-glycans in WM115

dx.doi.org/10.1021/pr401015b | J. Proteome Res. 2014, 13, 1021–1033

Table 1. List of *N*-Glycans Expressed on WM266-4 and WM115 Cells

no.	structure[a]	observed m/z WM266-4/115	monosaccharide composition	relative abundances (%) to total *N*-glycans[b]											
				WM266-4 cells					sum of	WM115 cells					sum of
				(a)	(b)	(c)	(d)	(e)	(a-e)	(a)	(b)	(c)	(d)	(e)	(a-e)
1		1030.41/1030.34	$Man_3GlcNAc_2$-2AA	1.38	-	-	-	-	**1.38**	2.91	-	-	-	-	**2.91**
2		1176.42/1176.29	$Fuc_1Man_3GlcNAc_2$-2AA	5.12	-	-	-	-	**5.12**	5.70	-	-	-	-	**5.70**
3		1379.44/1379.52	$Fuc_1Man_3GlcNAc_3$-2AA	1.18	-	-	-	-	**1.18**	3.84	-	-	-	-	**3.84**
4		1192.42/1192.49	$Man_4GlcNAc_2$-2AA	1.19	-	-	-	-	**1.19**	3.81	-	-	-	-	**0.42**
5		1338.39/1338.52	$Fuc_1Man_4GlcNAc_2$-2AA	0.59	-	-	-	-	**0.59**	0.42	-	-	-	-	**0.42**
6		1395.38/1395.37	$Gal_1Man_3GlcNAc_3$-2AA	0.44	0.99	-	-	-	**1.43**	0.53	1.78	-	-	-	**2.31**
7		1436.44/1436.51	$Man_3GlcNAc_4$-2AA	0.43	-	-	-	-	**0.43**	0.50	-	-	-	-	**0.50**
8		1354.35/1354.34	$Man_5GlcNAc_2$-2AA	6.50	-	-	-	-	**6.50**	13.68	-	-	-	-	**13.68**
9		1639.49/1639.38	$Man_3GlcNAc_5$-2AA	0.39	-	-	-	-	**0.39**	-	-	-	-	-	-
10		1744.49/1744.62	$Gal_1Fuc_1Man_3GlcNAc_4$-2AA	0.47	0.49	-	-	-	**0.96**	1.58	-	-	-	-	**1.58**
11		1516.40/1516.28	$Man_6GlcNAc_2$-2AA	17.14	-	-	-	-	**17.14**	13.60	-	-	-	-	**13.60**
12		1907.00/1906.85	$Gal_2Fuc_1Man_3GlcNAc_4$-2AA	0.43	4.03	4.73	-	-	**9.19**	0.59	6.10	4.29	-	-	**10.98**
13		1678.55/1678.39	$Man_7GlcNAc_2$-2AA	11.23	-	-	-	-	**11.23**	6.29	-	-	-	-	**6.29**
14		1840.55/1840.51	$Man_8GlcNAc_2$-2AA	8.47	-	-	-	-	**8.47**	7.05	-	-	-	-	**7.05**
15		2003.12/2002.98	$Man_9GlcNAc_2$-2AA	6.70	-	-	-	-	**6.70**	5.36	-	-	-	-	**5.36**
16		2166.59/2166.66	$Gal_2Man_3GlcNAc_6$-2AA	0.43	-	-	-	-	**0.43**	0.17	-	-	-	-	**0.17**
17		1541.35/1541.48	$Gal_1Fuc_1Man_3GlcNAc_3$-2AA	1.48	-	-	-	-	**1.48**	1.62	-	-	-	-	**1.62**
18		1703.45/1703.33	$Gal_1Fuc_1Man_4GlcNAc_3$-2AA	0.48	-	-	-	-	**0.48**	-	-	-	-	-	-
19		1598.55/1598.50	$Gal_1Man_3GlcNAc_4$-2AA	-	-	-	-	-	-	0.93	-	-	-	-	**0.93**
20		1760.41/1760.34	$Gal_2Man_3GlcNAc_4$-2AA	-	2.62	1.40	-	-	**4.02**	-	2.72	1.37	-	-	**4.09**
21		1719.48/1719.61	$Gal_1Man_5GlcNAc_3$-2AA	0.42	-	-	-	-	**0.42**	-	-	-	-	-	-
22		2109.39/2109.28	$Gal_2Fuc_1Man_3GlcNAc_5$-2AA	0.32	-	-	-	-	**0.32**	0.35	-	-	-	-	**0.35**
23		1865.44/1865.29	$Gal_1Fuc_1Man_5GlcNAc_3$-2AA	0.31	-	-	-	-	**0.31**	0.33	-	-	-	-	**0.33**
24		2125.39/2125.44	$Gal_3Man_3GlcNAc_5$-2AA	-	0.24	0.55	0.68	-	**1.47**	-	0.54	0.71	1.45	-	**2.70**
25		1881.47/1881.44	$Gal_1Man_6GlcNAc_3$-2AA	-	0.25	-	-	-	**0.25**	-	-	-	-	-	-
26		2271.35/2271.45	$Gal_3Fuc_1Man_3GlcNAc_5$-2AA	-	0.92	0.49	2.76	-	**4.17**	-	0.85	0.33	2.42	-	**3.60**
27		2474.69/2474.53	$Gal_3Fuc_1Man_3GlcNAc_6$-2AA	-	-	-	-	-	-	-	0.15	-	-	-	**0.15**
28		2490.98/2491.02	$Gal_4Man_3GlcNAc_6$-2AA	-	0.14	-	0.31	-	**0.45**	-	-	-	0.38	-	**0.38**
29		2636.44/2636.36	$Gal_4Fuc_1Man_3GlcNAc_6$-2AA	-	0.35	0.92	3.44	2.10	**6.81**	-	0.69	0.60	2.76	2.02	**6.07**
30	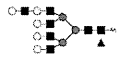	3003.04/3002.59	$Gal_5Fuc_1Man_3GlcNAc_7$-2AA	-	0.07	0.32	1.81	0.80	**3.00**	-	0.06	0.12	0.53	0.14	**0.85**

dx.doi.org/10.1021/pr401015b | *J. Proteome Res.* 2014, 13, 1021−1033

Table 1. continued

no.	structure[a]	observed m/z WM266-4/115	monosaccharide composition	relative abundances (%) to total *N*-glycans[b]											
				WM266-4 cells					sum of	WM115 cells					sum of
				(a)	(b)	(c)	(d)	(e)	(a-e)	(a)	(b)	(c)	(d)	(e)	(a-e)
31		3367.02/3366.78	$Gal_6Fuc_1Man_3GlcNAc_8$-2AA	-	0.04	0.16	1.18	0.48	**1.86**	-	-	0.09	0.36	0.06	**0.51**
32		3732.00/3732.34	$Gal_7Fuc_1Man_3GlcNAc_9$-2AA	-	-	0.11	0.87	0.30	**1.28**	-	-	0.05	0.19	-	**0.24**
33	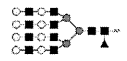	4097.92/4098.21	$Gal_8Fuc_1Man_3GlcNAc_{10}$-2AA	-	-	0.07	0.56	0.13	**0.76**	-	-	0.03	0.09	-	**0.12**
34	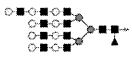	4462.07/4462.34	$Gal_9Fuc_1Man_3GlcNAc_{11}$-2AA	-	-	0.05	0.25	0.04	**0.34**	-	-	-	-	-	-
35	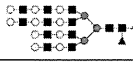	4827.69/4827.31	$Gal_{10}Fuc_1Man_3GlcNAc_{12}$-2AA	-	-	0.04	0.14	-	**0.18**	-	-	-	-	-	-

[*1]Structures of *N*-glycans were assigned based on the monosaccharide composition. [*2]Relative abundances (%) to total *N*-glycans were calculated as the ratios of individual *N*-glycans observed in five fractions. (a) Asialo-/highmannose-, (b) monosialo-, (c) disialo-, (d) trisialo-, and (e) tetrasialo-fraction. Abbreviations: Gal, galactose; Man, mannose; Fuc, fucose; GlcNAc, N-acetylglucosamine. Symbols: light gray-filled circle, Gal; gray-filled circle, Man; black-filled square, GlcNAc; black-filled triangle, Fuc.

cells were slightly higher than those (16.0 ± 2.8%) of WM266-4 cells. In contrast, disialo (peak c), trisialo (peak d), and tetrasialo (peak e) *N*-glycans in WM266-4 were present more abundantly than those in WM115 cells.

The glycan groups thus separated were further analyzed by NP-HPLC as asialo-*N*-glycans to improve resolutions among peaks. In asialo-/high-mannose fractions, a large amount of high-mannose type *N*-glycans were found as major constituents in both cells (Figure 2). Each peak was collected and analyzed by mass spectrometry and assigned as listed in Table 1.

Peaks **1**, **4**, **8**, **11**, **13**, **14**, and **15** were due to high-mannose type *N*-glycans having 3, 4, 5, 6, 7, 8, and 9 mannose residues. Structures of these *N*-glycans were easily confirmed by comparison with the standard samples obtained from RNase B and by combination of Jackbean α-mannosidase digestion and MALDI-TOF MS analysis. Elution positions of peaks **8**, **11**, **13**, **14**, and **15** were the same with those of five high-mannose-type *N*-glycans (Man5, 6, 7, 8, and 9) prepared from RNase B which contains only high-mannose-type glycans. Furthermore, when asialo-/high-mannose fractions (peak a) were digested with Jackbean α-mannosidase, peaks **1**, **4**, **8**, **11**, **13**, **14**, and **15** completely disappeared. These data clearly indicate that these peaks were due to high-mannose-type *N*-glycans.

After neuraminidase digestion of sialic acid-containing *N*-glycan fractions (peaks b, c, d, and e in Figure 1), the mixture of desialylated *N*-glycans from each fraction was analyzed in the same manner. In monosialo fractions, peaks **12** and **20**, which showed molecular ions at *m/z* 1907.00/1906.85 and 1760.41/1760.34, respectively, were abundantly present in both melanoma cells and are due to monofucosylated diantennary *N*-glycan and diantennary *N*-glycan, respectively. **18**, **21**, **25**, and **28** were observed only in WM266-4 cells, but **19** and **27** were observed only in WM115 cells. In disialo fractions, the major *N*-glycan **12** observed at 24 min showed a molecular ion at *m/z* 1907.00/1906.85 that was due to monofucosylated diantennary *N*-glycan. **12**, **26**, and **29** were observed commonly in WM266-4 and WM115 cells and assigned as monofucosylated diantennary, triantennary, and tetraantennary *N*-glycans, respectively. A small amount of tetraantennary *N*-glycans (**30**, **31**, **32**, and **33**), having one to four additional LacNAc (Gal-GlcNAc) residues, were observed in both melanoma cells as characteristic ladder peaks. In trisialo fractions, triantennary *N*-glycans (**24** and **26**) and tetraantennary *N*-glycans (**29**) were commonly observed in both WM266-4 and WM115 cells. Tetraantennary *N*-glycans derived from WM266-4 cells showed larger amount of ladder peaks (**30**, **31**, **32**, and **33**) between 30 and 35 min than those in WM115 cells. Also, *N*-glycans (**34** and **35**) having higher molecular weights were also detected only in WM266-4 cells. These ladder peaks (peaks **30**–**35**) were due to tetraantennary *N*-glycans having different numbers of LacNAc residues. For example, *N*-glycans (**34** and **35**) showed molecular ions at *m/z* 4462 and 4827, respectively, and were assigned as tetraantennary *N*-glycans having five and six LacNAc residues at the nonreducing terminal ends (Supporting Information Figure S1). Although *N*-glycans having small numbers of polyLacNAc residues (**30**, **31**, **32**, and **33**) were also observed in WM115 cells, their relative abundances to total *N*-glycans were significantly lower than those in WM266–4 cells. In tetrasialo fractions, monofucosylated tetraantennary *N*-glycan (**29**) was the major glycan observed in both cells. Tetraannattenary *N*-glycans substituted with multiple polylactosamine residues (**32**, **33**, and **34**) were observed only in WM266–4 cells.

In summary, we identified 35 *N*-glycans (as asialo *N*-glycans) as shown in Table 1. Most of the complex-type *N*-glycans were commonly observed in both WM266-4 and WM115 cells. Typical complex-type *N*-glycans with one Fuc residue (**12**, **26**, and **29**) were abundantly observed in both melanoma cells, and the sum of relative abundances of these glycans in WM266-4/WM115 cells were 9.19%/10.98% (**12**), 4.17%/3.60% (**26**), and 6.81%/6.07% (**29**), respectively. These results indicate that there are no remarkable difference in the biosynthetic machinery for core structure of bi- (**12**, **20**), tri- (**24**, **26**), and tetra-antennary (**28**, **29**) *N*-glycans. In contrast, expression levels of polyLacNAc-carrying *N*-glycans (**30**, **31**, **32**, and **33**) were significantly higher in WM266-4 cells. The sum of relative abundances of **30** and **31** in WM266-4 were 3.5-fold higher than those in WM115. Also, relative abundances of **32** and **33** were markedly higher in WM266-4 cells. PolyLacNAc-carrying *N*-glycans with additional LacNAc residues (**34** and **35**) were observed only in WM266-4 cells. Thus, polyLacNAc-carrying *N*-glycans were abundantly expressed in metastatic melanoma cells (WM266-4) as compared with primary melanoma cells (WM115). The expression level of polylactosamine-type *N*-

dx.doi.org/10.1021/pr401015b | *J. Proteome Res.* 2014, 13, 1021–1033

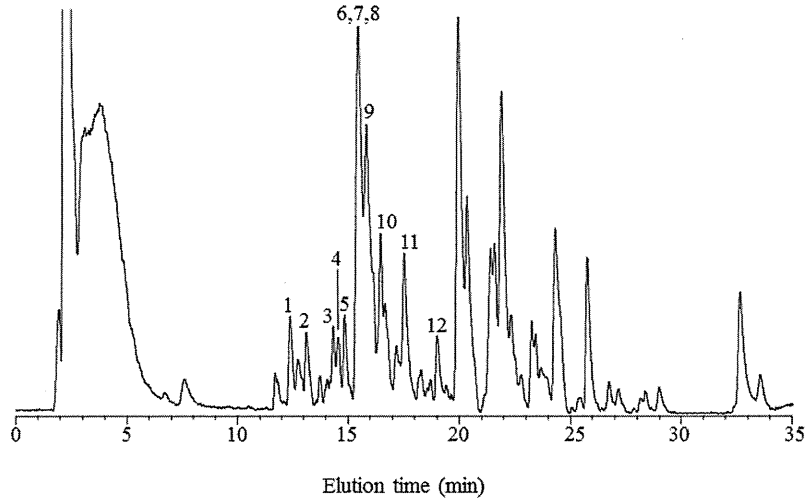

Figure 3. Total ion chromatogram of DSA-bound glycopeptides. Analytical conditions: see Materials and Methods. Peak numbers correspond to those in the list of Table 2

Table 2. Glycoproteins Having Polylactosamine-Carrying *N*-Glycans Identified in WM266-4 Cells

peptide no.	protein name	MW (kDa)	precursor ions	error (Da)	score	peptide sequence[a,b]
1	CD63 antigen	25.6	$[M + 2H]^{2+}$ = 738.30	0.02	25	CCGAANYTDWEK
2	CD109 antigen	161.7	$[M + 2H]^{2+}$ = 706.36	0.02	26	TQDEILFSNSTR
3	cell adhesion molecule 1	48.5	$[M + 2H]^{2+}$ = 689.37	0.02	39	VSLTNVSISDEGR
4	chondroitin sulfate proteoglycan 4 (CSPG4)	250.5	$[M + 2H]^{2+}$ = 644.36	0.01	71	GVNASAVVNVTVR
5	CD59 antigen	14.5	$[M + 2H]^{2+}$ = 901.92	0.02	78	TAVNCSSDFDACLITK
6	CD63 antigen	25.6	$[M + 2H]^{2+}$ = 707.00	0.07	23	CCGAANYTDWEKIPSMSK
7	CD63 antigen	25.6	$[M + 2H]^{2+}$ = 852.07	0.03	67	NRVPDSCCINVTGCGINFNEK
8	basigin (CD147)	42.2	$[M + 3H]^{3+}$ = 663.35	0.03	50	ILLTCSLNDSATEVTGHR
9	chondroitin sulfate proteoglycan 4 (CSPG4)	250.5	$[M + 2H]^{2+}$ = 742.91	0.02	70	LDPTVLDAGELANR
10	lysosome-associated membrane glycoprotein-1	44.9	$[M + 3H]^{3+}$ = 721.71	0.03	62	SGPKNMTFDLPSDATVVLNR
11	lysosome-associated membrane glycoprotein-1	44.9	$[M + 2H]^{2+}$ = 897.97	0.02	34	NMTFDLPSDATVVLNR
12	chondroitin sulfate proteoglycan 4 (CSPG4)	250.5	$[M + 3H]^{3+}$ = 897.09	0.06	40	YVHDGSETLTDSFVLMANASEMDR

[a]Sequences marked with underline are by the *N*-glycosylation potential sites (Asn-X-Ser/Thr). [b]All cysteine residues are modified with carbamidomethylation.

glycans may be correlated with expression level of β1-6*N*-acetyl-glucosamine (β1-6GlcNAc), and β1-6 GlcNAc branching on *N*-glycans is increased in malignant transformation in cancer metastasis.[23−25] Some groups reported *N*-glycosylation patterns in human melanoma cells at different progression stages by lectin-blotting analysis using *Phaseolus vulgaris*-leucoagglutinin (PHA-L) which recognizes β1-6GlcNAc branch on Manα1-6 branch of *N*-glycans and demonstrated that β1-6GlcNAc-expressing glycoproteins were abundantly observed in metastatic melanoma cells (e.g., WM239, WM9, and A375).[26,27] It is well-known that *N*-acetylglucosaminyltransferase-V (GnT-V, *Mgat5*) catalyzes the transfer of GlcNAc to the OH-6 position of the Man residue in Manα1-6Man branch of trimannosyl core structure and higher expression of this enzyme has been shown to induce metastatic spread.[24] Difference in expression level of polylactosamine-type *N*-glycans may be due to the difference in expression level of GnT-V between both cells. These data prompted us to find specific protein(s) expressing *N*-glycans having multiple polylactosamine-type residues that were observed in WM266-4.

Identification of Glycoproteins Carrying PolyLacNAc Residues in WM266-4 Cells

We previously found that integrin-α5 (CD49e), carcinoembryonic antigen (CEA)-related cell adhesion molecule 5 (CD66e), CD107a, and CD107b were common glycoproteins carrying polyLacNAc-type *N*-glycans in histiocytic lymphoma cells (U937) and gastric cancer cells (MKN45).[18] These glycoproteins were confirmed as follows: (i) capturing of glycopeptides by characteristic glycan-recognizing lectin(s), (ii) analysis of the released glycans from the captured glycopeptides after *N*-glycoamidase F, and (iii) LC/MS of the peptides having *N*-glycosylation sites.

In the similar manner employed in the previous studies, whole protein from WM266-4 cells was digested with TPCK-trypsin, and polyLacNAc-carrying glycopeptides were collected using a *Datura stramonium* agglutinin (DSA)-immobilized agarose column[18] (Supporting Information Figure S2 and Table S1). It is known that DSA shows specificity to β1−4 linked oligomers of GlcNAc and also shows affinity to polyLacNAc residues on glycoconjugates.[18] The collected DSA-bound glycopeptides were digested with *N*-glycoamidase F, and the mixtures of peptides after releasing *N*-glycans thus obtained were analyzed by LCMS (Figure 3). More than 30 peaks were observed on the total ion chromatogram. The peaks

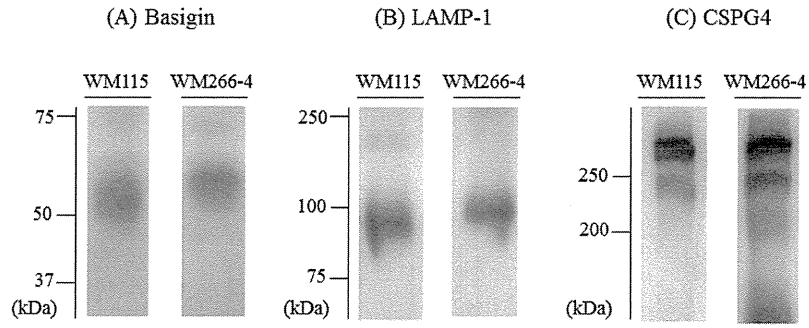

Figure 4. Western blot analysis of glycoproteins containing polyLacNAc residues commonly present in WM266-4 and WM115 cells. Analytical conditions: separation gel, 10% T/2.6% C; blotting buffer, 48 mM Tris-39 mM glycine–20% methanol; blocking buffer for lectin blot, 0.05% Tween 20 in PBS; blocking buffer for Western blot, 5% skim milk–0.05% Tween 20 in PBS. Detection: HRP-DAB.

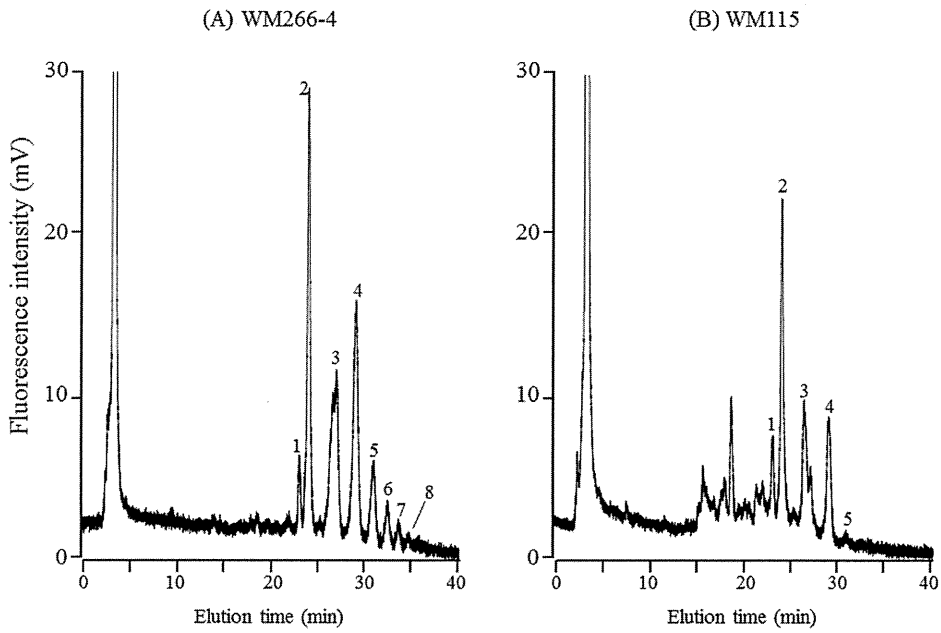

Figure 5. Analysis of *N*-glycans expressed on CSPG4 in WM266-4 (A) and WM115 (B) cells. The *N*-glycans were previously digested with neuraminidase. Analytical conditions are the same as in Figure 2. The *m/z* values and structures of individual peaks were summarized in Table 3. Structures corresponding to the peak numbers are summarized in Table 3

observed from 11 to 19 min showed molecular ions from *m/z* 500 to *m/z* 1000 (charge state: +2 or +3) (Supporting Information Table S2). On the other hand, peaks appeared later than 20 min showed low molecular ions (less than *m/z* 500). The small peptides have little information on peptide sequences. Therefore, the peaks observed from 11 to 19 min were analyzed by MS/MS technique, and 12 peptides were proved to have Asn-X-Ser/Thr consensus sequence for *N*-glycosylation site as shown in Table 2 (Supporting Information Figure S3, Table S2, and Table S3).

The sequences of CCGAANYTDWEK (**1**), CCGAANYTDWEKIPSMSK (**6**), and NRVPDSCCINVTGCGINFNEK (**7**) were assinged to the sequences of CD63 (CD63_HUMAN:P08962). The presence of polyLacNAc-type *N*-glycans in CD63 of human melanoma cells was already reported.[28] Three peptide sequences (**4**, **9**, and **12** for GVNASAVVNVTVR, LDPTVLDAGELANR, and YVHDGSETLTDSFVLMANASEMDR, respectively) were due to chondroitin sulfate proteoglycan 4 (CSPG4_HUMAN:Q6UVK1). CSPG4 is a high molecular weight glycoprotein having both *N*-glycans and CS chains, although the presence of polyLacNAc-type *N*-glycans in CSPG4 has not been reported.

Peptides **10** (SGPKNMTFDLPSDATVVLNR) and **11** (NMTFDLPSDATVVLNR) corresponded to the sequences for lysosome-associated membrane glycoprotein-1 (LAMP1_HUMAN:P11279). *N*-Glycans on LAMP-1 in various cells are often modified with polyLacNAc.[29−31] We also reported that LAMP-1 in some cancer cells contained a large amount of *N*-glycans having polyLacNAc.[18] Basigin (BASI_HUMAN:P35613) as well as LAMP-1 are glycoproteins having polyLacNAc-type *N*-glycans.[29−31] Krishnan et al. also reported that the immunoprecipitated LAMP-1from the cell lysates of mouse high metastatic melanoma cells (B16F10) express higher levels of polyLacNAc-type glycans than those of low metastatic melanoma cells (B16F1).[32] The results are well consistent with our present findings. Other sequences (**2**, **3**, and **5**) were due to CD109 (CD109_HUMAN:Q6YHK3), cell adhesion molecule 1 (CADM1_HUMAN:Q9BY67), and CD59 (CD59_HUMAN:P13987), respectively.

These proteins having polyLacNAc-type-*N*-glycans were further confirmed by Western blot analysis (Figure 4).

Basigin was detected at 50–60 kDa (Figure 4A) in both cells. LAMP-1 is composed of 417 amino acids and observed at ca. 100 kDa (Figure 4B) also in both cells. LAMP-1 is a highly

Table 3. List of *N*-Glycans Observed in CSPG4 Derived from WM266-4 and WM115 Cells[a]

peak no.	observed m/z		monosaccharide composition	structure	relative abundances[b] (mean ± SD; n=3)	
	WM266-4	WM115			WM266-4	WM115
1	1760.70	1761.15	$Gal_2Man_3GlcNAc_4$-2AA	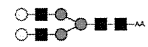	10.3±4.6%	11.9±1.1%
2	1907.21	1907.26	$Gal_2Fuc_1Man_3GlcNAc_4$-2AA	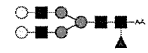	38.7±1.0%	47.7±3.5%
3	2272.27	2272.19	$Gal_3Fuc_1Man_3GlcNAc_5$-2AA	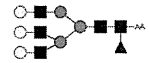	14.3±4.9%	19.8±0.7%
4	2637.59	2637.14	$Gal_4Fuc_1Man_3GlcNAc_6$-2AA	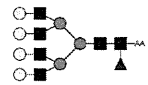	20.8±2.6%	18.5±3.2%
5	3002.75	3003.25	$Gal_5Fuc_1Man_3GlcNAc_7$-2AA	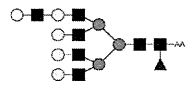	7.4±1.4%	2.1±1.3%
6	3367.85	n.d.[c]	$Gal_6Fuc_1Man_3GlcNAc_8$-2AA	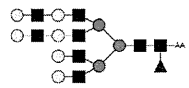	4.2±2.3%	-
7	3733.25	n.d.[c]	$Gal_7Fuc_1Man_3GlcNAc_9$-2AA	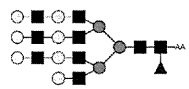	3.0±2.8%	-
8	4098.56	n.d.[c]	$Gal_8Fuc_1Man_3GlcNAc_{10}$-2AA	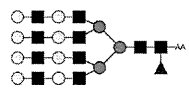	1.3±1.0%	-

[a]Abbreviations: Gal, galactose; Man, mannose; Fuc, fucose; GlcNAc, *N*-acetylglucosamine. Symbols: light gray-filled circle, Gal; gray-filled circle, Man; black-filled square, GlcNAc; black-filled triangle, Fuc. [b]Relative abundances were calculated as ratios of individual *N*-glycans to total *N*-glycans expressed in CSPG4. [c]Not detected.

glycosylated protein, having 18 *N*-glycosylation cites and also 4 *O*-glycosylation sites.[33] Basigin and LAMP-1 in WM266-4 cells showed slightly larger molecular sizes than those in WM115 cells. The difference in molecular sizes of these glycoproteins may be due to molecular sizes of attached *N*-glycans because polyLacNAc-type *N*-glycans are more abundantly expressed in WM266-4 cells as shown in Table 1. CSPG4 was observed at >250 kDa (Figure 4C). Although core protein of CSPG4 is composed of 2322 amino acids, the observed large molecular size is due to the presence of 15 *N*-glycans and a chondroitin sulfate (CS) chain.[34] CD63, of which presence was confirmed by LC/MS, could not be detected in WM115 cells by Western blot analysis (data not shown). Among these glycoproteins commonly observed in WM266-4 and WM115 cells, CSPG4 in melanoma cells has been reported to be a melanoma specific antigen.[35] CS chains in CSPG4 molecule are involved in various biological functions such as cell adhesion, cell invasion, and cell angiogenesis.[36−38] Fukushi et al. reported that CSPG4 promotes cell motility and angiogenesis via interaction with galectin-3 which is the endogenous polyLacNAc-binding protein.[38] CS chains on CSPG4 regulate matrix metalloproteinase (MMP)-dependent human melanoma invasion.[39] Thus, changes in glycosylation during malignant transformation and tumor progression (i.e., difference in glycan profiles between WM115 cells and WM266-4 cells) should have some correlation with physiological states of these cells. However, detailed information on structures of *N*-glycans and chondroitin sulfate attached to the core protein of CSPG4 is not available.

N-Glycans of CSPG4 Obtained from WM266-4 and WM115 Cells by Immunoprecipitation Method

As shown in Figure 5, both cells showed similar *N*-glycan profiles. However, relative abundances of *N*-glycans were significantly different between WM266-4 and WM115 cells.

CSPG4 expressed in WM266-4 cells contained a large amount of polyLacNAc-type *N*-glycans (15.9% for peaks **5**, **6**, **7**, and **8**), and the relative abundance was ca. 7.5-fold higher than that of WM115 cells. In WM115 cells, typical complex-type *N*-glycans (i.e., biantennary (**1** and **2**)-, triantennary (**3**)-, and tetraantennary (**4**)-glycans) were observed as the major glycans. The sum of these typical complex-type *N*-glycans (**1**−**4**) was 97.9% in total *N*-glycans, and the relative abundance of polyLacNAc-type *N*-glycans was very low (2.1%). Oncogene activation often stimulates expression of the Golgi enzymes that are responsible for the synthesis of polyLacNAc-type *N*-glycans.[40,41] PolyLacNAc-type *N*-glycans, which are found on proteins such as growth factor receptors and integrins, are shown to enhance growth signaling in motile tumor cells.[42] It was also reported that polyLacNAc-type *N*-glycan levels were increased in highly metastatic tumor cell lines.[32,43] Krishnan et al. investigated the biological roles of polyLAcNAc residues on organ specific metastasis and revealed that high metastatic melanoma cell, expressing high level of polyLAcNAc-*N*-glycans, show high affinity to the galectin-3-expressed lung vascular endothelium.[32] The increased level of polyLacNAc-type *N*-glycans may change cell adhesion through carbohydrate−lectin interaction, resulting in facilitating tumor cell invasion and metastasis.[44] The present data, which show higher expression of polyLacNAc-type *N*-glycans in metastatic WM266-4 cells, support these previously reported results.

dx.doi.org/10.1021/pr401015b | *J. Proteome Res.* 2014, 13, 1021−1033

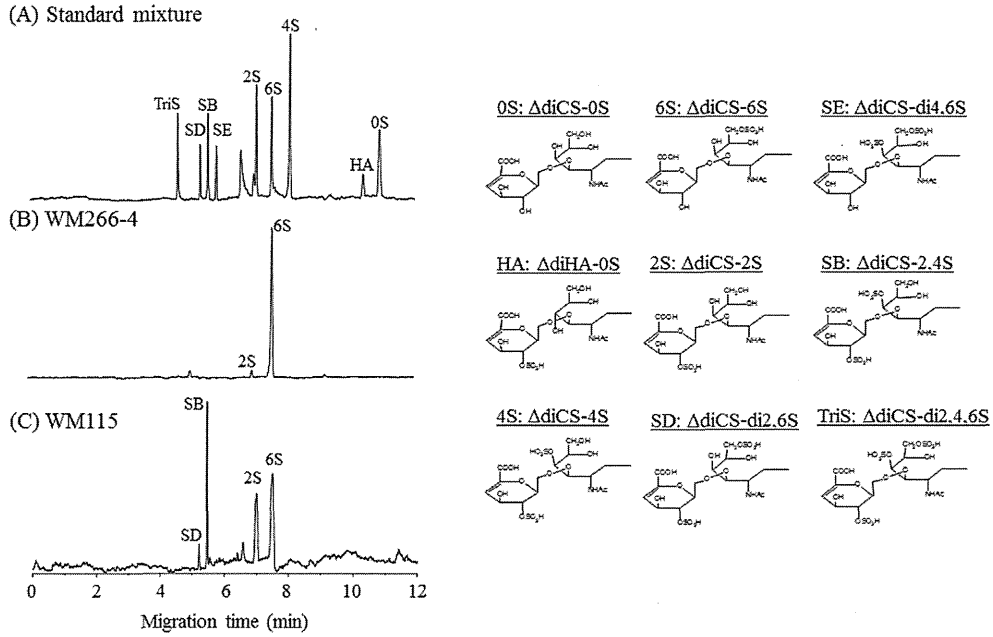

Figure 6. Analysis of unsaturated disaccharides expressed on CSPG4 in WM266-4 and WM115 cells and structures of unsaturated disaccharides from chondroitin sulfate/hyaluronic acid. (A) standard mixture of nine unsaturated disaccharides. (B and C) Results on digestion of CSPG4 with chondroitinase ABC. Analytical conditions: capillary, fused silica capillary (50 μm i.d., 30 cm); running buffer, 0.1 M Tris-phosphate buffer (pH 3.0); applied voltage, −25 kV; injection, pressure injection (1.0 psi, 5s); temperature, 25 °C; detection, He−Cd laser-induced fluorescent detection (excitation 325 nm, emission 405 nm).

Analysis of Chondroitin Sulfate of CSPG4 Obtained from WM266-4 and WM115 Cells

Alterations in sulfation pattern of CS chains have been reported in relation to malignant transformation and progression.[45−47] Human gastric carcinoma-derived versican, which is a high molecular weight chondroitin sulfate proteoglycan, showed increase of 6-sulfated CS chains with parallel decrease of 4-sulfated CS chains as compared to human normal gastric mucosa.[46] Iida et al. reported that chondroitin 4-sulfate expressed on melanoma cells activated matrix metalloproteinase-2 (MMP-2) and enhanced cell invasion and metastasis.[48]

We performed comparative analysis of CS chains on CSPG4 derived from WM266-4 and WM115 cells. Another portion of CSPG4 used for the analysis of *N*-glycans as described above was digested with chondroitinase ABC, and the eliminated unsaturated disaccharides was labeled with 2-AA[22] and analyzed by laser-induced fluorescence detection (LIF)-CE (Figure 6).

WM266-4 cells showed simple profiles and contained ΔdiCS-6S (6S) as the major component and ΔdiCS-2S (2S) as the minor one. Disulfated unsaturated disaccharides such as SD, SE, and SB were not detected. In contrast, four unsaturated disaccharides, ΔdiCS-2S (2S), ΔdiCS-6S (6S), ΔdiCS-di2,4S (SB), and ΔdiCS-di2,6S (SD), were observed in WM115 cells. Disulfated unsaturated disaccharides (SB and SD), which are abundantly present in dermatan sulfate (DS), were observed only in WM115 cells. It should be noticed that ΔdiCS-4S (4S) given from chondroitin 4-sulfate (CS4) was not detected in both melanoma cells. Iida et al. reported that CSPG4 is decorated with CS4 in human melanoma.[48] Our present data are quite different, with their report indicating that CS4 is the major component of CSPG4 in melanoma cell lines.[48−50] CS chains on CSPG4 is believed to be important for their biological functions such as activation of matrix metlalloproteinase, activation of integrin, or cell surface localization.[37,48,51] Recent studies have also reported that CSPG4 enhanced activation of integrin-related signal transduction pathways, which may be an important role on tumor progression.[52,53] Although how or whether tumor-associated changes in the sulfation patterns (e.g., chondroitin-6-sulfation) and CS chain extension on CSPG4 occur is currently unknown, metastasis-associated changes in CS modification on CSPG4 may facilitate migration and invasion.

CONCLUSION

In the present study, we performed comparative analysis of glycoproteins expressed commonly in the matched patient primary and metastatic melanoma cell lines. Although most of the complex-type *N*-glycans were commonly observed in both primary and metastatic melanoma cells (WM115 and WM266-4 cells, respectively), expression level of polyLacNAc-carrying *N*-glycans was significantly higher in WM266-4 cells, and we found that expression of polyLacNAc-carrying *N*-glycans was preferentially due to LAMP-1, CD63, Basigin, and CSPG4 as examined by a combination of lectin affinity chromatography and LC/MS-based proteomics approaches. Among the identified glycoproteins, CSPG4 is a well-known marker for melanoma, and we found that the expression level of polyLacNAc-carrying *N*-glycans in metastatic melanoma (WM266-4) was significantly higher than those in primary melanoma (WM115). The results are in good agreement with the reports describing that polyLacNAc-carrying *N*-glycans are increased in malignant transformation in cancer metastasis.[23−27]

Sulfation patterns of chondroitin sulfate chain in CSPG4 showed distinct changes between primary and metastatic melanoma cells. In WM266-4 cells, ΔdiCS-6S (6S) was the major component. In contrast, WM115 showed relatively complex unsaturated disaccharide profiles, and four unsaturated disaccharides, ΔdiCS-2S (2S), ΔdiCS-6S (6S), ΔdiCS-di2,4S (SB), and ΔdiCS-di2,6S (SD) as the major components, were

dx.doi.org/10.1021/pr401015b | J. Proteome Res. 2014, 13, 1021−1033

observed in WM115 cells. It should be noticed that the present results were inconsistent with the previous reports that CSPG4 was mainly decorated with chondroitin 4-sulfate in human melanomas.[48,49]

In conclusion, post-translational modification of a protein with carbohydrates in melanoma cells becomes quite different with malignant transformation in acquiring metastasis ability, and glycans attached to tumor-specific cells are distinctively different with changes of their physiological state such as metastasis ability. Although further studies are required, comparative analyses of glycans attached to disease-specific glycoproteins will lead to develop new markers for determination of the degree of malignancy.

■ ASSOCIATED CONTENT

Supporting Information

MS/MS spectra of polyLacNAc-type *N*-glycans observed in WM266-4 cells, NP-HPLC analysis of *N*-glycan on glycopeptides fractionate by DSA-agarose column, MSMS spectra of deglycosylated peptides captured by DSA-agarose (PDF); summary of *N*-glycans on glycopeptides fractionated by DSA-agarose column, summary of MS analysis of deglycosylated peptides captured by DSA-agarose column, summary of MSMS analysis of glycopeptides captured by DSA-agarose column (XLSX). This material is available free of charge via the Internet at http://pubs.acs.org.

■ AUTHOR INFORMATION

Corresponding Author

*Phone: +80-6-6730-5880 ext 3868. Fax: +80-6-6730-1394. E-mail:k_kakehi@phar.kindai.ac.jp.

Notes

The authors declare no competing financial interest.

■ REFERENCES

(1) Helenius, A.; Aebi, M. Intracellular functions of N-linked glycans. *Science* **2001**, *291* (5512), 2364–2369.

(2) Parodi, A. J. Protein glucosylation and its role in protein folding. *Annu. Rev. Biochem.* **2000**, *69*, 69–93.

(3) Angata, T.; Fujinawa, R.; Kurimoto, A.; Nakajima, K.; Kato, M.; Takamatsu, S.; Korekane, H.; Gao, C. X.; Ohtsubo, K.; Kitazume, S.; Taniguchi, N. Integrated approach toward the discovery of glycobiomarkers of inflammation-related diseases. *Ann. N. Y. Acad. Sci.* **2012**, *1253*, 159–169.

(4) Drake, P. M.; Cho, W.; Li, B.; Prakobphol, A.; Johansen, E.; Anderson, N. L.; Regnier, F. E.; Gibson, B. W.; Fisher, S. J. Sweetening the pot: adding glycosylation to the biomarker discovery equation. *Clin. Chem.* **2009**, *56* (2), 223–236.

(5) Fuster, M. M.; Esko, J. D. The sweet and sour of cancer: glycans as novel therapeutic targets. *Nature Rev. Cancer* **2005**, *5* (7), 526–542.

(6) Narimatsu, H.; Sawaki, H.; Kuno, A.; Kaji, H.; Ito, H.; Ikehara, Y. A strategy for discovery of cancer glyco-biomarkers in serum using newly developed technologies for glycoproteomics. *FEBS J.* **2009**, *277* (1), 95–105.

(7) Tharmalingam, T.; Marino, K.; Rudd, P. M. Platform technology to identify potential disease markers and establish heritability and environmental determinants of the human serum *N*-glycome. *Carbohydr. Res.* **2010**, *345* (10), 1280–1282.

(8) Kannagi, R.; Fukushi, Y.; Tachikawa, T.; Noda, A.; Shin, S.; Shigeta, K.; Hiraiwa, N.; Fukuda, Y.; Inamoto, T.; Hakomori, S.; et al. Quantitative and qualitative characterization of human cancer-associated serum glycoprotein antigens expressing fucosyl or sialylfucosyl type 2 chain polylactosamine. *Cancer Res.* **1986**, *46* (5), 2619–2626.

(9) Korczak, B.; Goss, P.; Fernandez, B.; Baker, M.; Dennis, J. W. Branching N-linked oligosaccharides in breast cancer. *Adv. Exp. Med. Biol.* **1994**, *353*, 95–104.

(10) Miyake, M.; Kohno, N.; Nudelman, E. D.; Hakomori, S. Human IgG3 monoclonal antibody directed to an unbranched repeating type 2 chain (Gal beta 1——4GlcNAc beta 1——3Gal beta 1——4GlcNAc beta 1——3Gal beta 1——R) which is highly expressed in colonic and hepatocellular carcinoma. *Cancer Res.* **1989**, *49* (20), 5689–5695.

(11) Zenita, K.; Kirihata, Y.; Kitahara, A.; Shigeta, K.; Higuchi, K.; Hirashima, K.; Murachi, T.; Miyake, M.; Takeda, T.; Kannagi, R. Fucosylated type-2 chain polylactosamine antigens in human lung cancer. *Int. J. Cancer* **1988**, *41* (3), 344–349.

(12) Sozzani, P.; Arisio, R.; Porpiglia, M.; Benedetto, C. Is Sialyl Lewis x antigen expression a prognostic factor in patients with breast cancer? *Int. J. Surg. Pathol.* **2008**, *16* (4), 365–374.

(13) Arnold, J. N.; Saldova, R.; Hamid, U. M.; Rudd, P. M. Evaluation of the serum N-linked glycome for the diagnosis of cancer and chronic inflammation. *Proteomics* **2008**, *8* (16), 3284–3293.

(14) Kim, Y. S.; Yoo, H. S.; Ko, J. H. Implication of aberrant glycosylation in cancer and use of lectin for cancer biomarker discovery. *Protein Pept. Lett.* **2009**, *16* (5), 499–507.

(15) Kuno, A.; Ikehara, Y.; Tanaka, Y.; Angata, T.; Unno, S.; Sogabe, M.; Ozaki, H.; Ito, K.; Hirabayashi, J.; Mizokami, M.; Narimatsu, H. Multilectin assay for detecting fibrosis-specific glyco-alteration by means of lectin microarray. *Clin. Chem.* **2011**, *57* (1), 48–56.

(16) Naka, R.; Kamoda, S.; Ishizuka, A.; Kinoshita, M.; Kakehi, K. Analysis of total *N*-glycans in cell membrane fractions of cancer cells using a combination of serotonin affinity chromatography and normal phase chromatography. *J. Proteome Res.* **2006**, *5* (1), 88–97.

(17) Yamada, K.; Kinoshita, M.; Hayakawa, T.; Nakaya, S.; Kakehi, K. Comparative studies on the structural features of *O*-glycans between leukemia and epithelial cell lines. *J. Proteome Res.* **2009**, *8* (2), 521–537.

(18) Mitsui, Y.; Yamada, K.; Hara, S.; Kinoshita, M.; Hayakawa, T.; Kakehi, K. Comparative studies on glycoproteins expressing polylactosamine-type *N*-glycans in cancer cells. *J. Pharm. Biomed. Anal.* **2012**, *70*, 718–726.

(19) Dickson, P. V.; Gershenwald, J. E. Staging and prognosis of cutaneous melanoma. *Surg. Oncol. Clin. N. Am.* **2011**, *20* (1), 1–17.

(20) Brochez, L.; Naeyaert, J. M. Serological markers for melanoma. *Br. J. Dermatol.* **2000**, *143* (2), 256–268.

(21) Kamoda, S.; Nakanishi, Y.; Kinoshita, M.; Ishikawa, R.; Kakehi, K. Analysis of glycoprotein-derived oligosaccharides in glycoproteins detected on two-dimensional gel by capillary electrophoresis using on-line concentration method. *J. Chromatogr., A* **2006**, *1106* (1–2), 67–74.

(22) Yamada, K.; Mitsui, Y.; Kakoi, N.; Kinoshita, M.; Hayakawa, T.; Kakehi, K. One-pot characterization of cancer cells by the analysis of mucin-type glycans and glycosaminoglycans. *Anal. Biochem.* **2012**, *421* (2), 595–606.

(23) Datti, A.; Donovan, R. S.; Korczak, B.; Dennis, J. W. A homogeneous cell-based assay to identify N-linked carbohydrate processing inhibitors. *Anal. Biochem.* **2000**, *280* (1), 137–142.

(24) Dennis, J. W.; Granovsky, M.; Warren, C. E. Glycoprotein glycosylation and cancer progression. *Biochim. Biophys. Acta* **1999**, *1473* (1), 21–34.

(25) Prokopishyn, N. L.; Puzon-McLaughlin, W.; Takada, Y.; Laferte, S. Integrin alpha3beta1 expressed by human colon cancer cells is a major carrier of oncodevelopmental carbohydrate epitopes. *J. Cell. Biochem.* **1999**, *72* (2), 189–209.

(26) Ciolczyk-Wierzbicka, D.; Gil, D.; Hoja-Lukowicz, D.; Litynska, A.; Laidler, P. Carbohydrate moieties of *N*-cadherin from human melanoma cell lines. *Acta Biochim. Pol.* **2002**, *49* (4), 991–998.

(27) Przybylo, M.; Martuszewska, D.; Pochec, E.; Hoja-Lukowicz, D.; Litynska, A. Identification of proteins bearing beta1–6 branched *N*-glycans in human melanoma cell lines from different progression stages by tandem mass spectrometry analysis. *Biochim. Biophys. Acta* **2007**, *1770* (9), 1427–1435.

(28) Engering, A.; Kuhn, L.; Fluitsma, D.; Hoefsmit, E.; Pieters, J. Differential post-translational modification of CD63 molecules during maturation of human dendritic cells. *Eur. J. Biochem.* **2003**, *270* (11), 2412–2420.

(29) Carlsson, S. R.; Fukuda, M. The polylactosaminoglycans of human lysosomal membrane glycoproteins lamp-1 and lamp-2. Localization on the peptide backbones. *J. Biol. Chem.* **1990**, *265* (33), 20488–20495.

(30) Laferte, S.; Dennis, J. W. Purification of two glycoproteins expressing beta 1–6 branched Asn-linked oligosaccharides from metastatic tumour cells. *Biochem. J.* **1989**, *259* (2), 569–576.

(31) Tang, W.; Chang, S. B.; Hemler, M. E. Links between CD147 function, glycosylation, and caveolin-1. *Mol. Biol. Cell* **2004**, *15* (9), 4043–4050.

(32) Krishnan, V.; Bane, S. M.; Kawle, P. D.; Naresh, K. N.; Kalraiya, R. D. Altered melanoma cell surface glycosylation mediates organ specific adhesion and metastasis via lectin receptors on the lung vascular endothelium. *Clin. Exp. Metastasis* **2005**, *22* (1), 11–24.

(33) Carlsson, S. R.; Lycksell, P. O.; Fukuda, M. Assignment of *O*-glycan attachment sites to the hinge-like regions of human lysosomal membrane glycoproteins lamp-1 and lamp-2. *Arch. Biochem. Biophys.* **1993**, *304* (1), 65–73.

(34) Hubbard, S. C.; Ivatt, R. J. Synthesis and processing of asparagine-linked oligosaccharides. *Annu. Rev. Biochem.* **1981**, *50*, 555–583.

(35) Pluschke, G.; Vanek, M.; Evans, A.; Dittmar, T.; Schmid, P.; Itin, P.; Filardo, E. J.; Reisfeld, R. A. Molecular cloning of a human melanoma-associated chondroitin sulfate proteoglycan. *Proc. Natl. Acad. Sci. U. S. A.* **1996**, *93* (18), 9710–9715.

(36) Eisenmann, K. M.; McCarthy, J. B.; Simpson, M. A.; Keely, P. J.; Guan, J. L.; Tachibana, K.; Lim, L.; Manser, E.; Furcht, L. T.; Iida, J. Melanoma chondroitin sulphate proteoglycan regulates cell spreading through Cdc42, Ack-1 and p130cas. *Nature Cell Biol.* **1999**, *1* (8), 507–513.

(37) Iida, J.; Meijne, A. M.; Oegema, T. R., Jr.; Yednock, T. A.; Kovach, N. L.; Furcht, L. T.; McCarthy, J. B. A role of chondroitin sulfate glycosaminoglycan binding site in alpha4beta1 integrin-mediated melanoma cell adhesion. *J. Biol. Chem.* **1998**, *273* (10), 5955–5962.

(38) Fukushi, J.; Makagiansar, I. T.; Stallcup, W. B. NG2 proteoglycan promotes endothelial cell motility and angiogenesis via engagement of galectin-3 and alpha3beta1 integrin. *Mol. Biol. Cell* **2004**, *15* (8), 3580–3590.

(39) Iida, J.; Pei, D.; Kang, T.; Simpson, M. A.; Herlyn, M.; Furcht, L. T.; McCarthy, J. B. Melanoma chondroitin sulfate proteoglycan regulates matrix metalloproteinase-dependent human melanoma invasion into type I collagen. *J. Biol. Chem.* **2001**, *276* (22), 18786–18794.

(40) Dennis, J. W.; Kosh, K.; Bryce, D. M.; Breitman, M. L. Oncogenes conferring metastatic potential induce increased branching of Asn-linked oligosaccharides in rat2 fibroblasts. *Oncogene* **1989**, *4* (7), 853–860.

(41) Dennis, J. W.; Laferte, S.; Waghorne, C.; Breitman, M. L.; Kerbel, R. S. Beta 1–6 branching of Asn-linked oligosaccharides is directly associated with metastasis. *Science* **1987**, *236* (4801), 582–585.

(42) Beheshti Zavareh, R.; Lau, K. S.; Hurren, R.; Datti, A.; Ashline, D. J.; Gronda, M.; Cheung, P.; Simpson, C. D.; Liu, W.; Wasylishen, A. R.; Boutros, P. C.; Shi, H.; Vengopal, A.; Jurisica, I.; Penn, L. Z.; Reinhold, V. N.; Ezzat, S.; Wrana, J.; Rose, D. R.; Schachter, H.; Dennis, J. W.; Schimmer, A. D. Inhibition of the sodium/potassium ATPase impairs *N*-glycan expression and function. *Cancer Res.* **2008**, *68* (16), 6688–6697.

(43) Gu, J.; Sato, Y.; Kariya, Y.; Isaji, T.; Taniguchi, N.; Fukuda, T. A mutual regulation between cell-cell adhesion and *N*-glycosylation: implication of the bisecting GlcNAc for biological functions. *J. Proteome Res.* **2009**, *8* (2), 431–435.

(44) Demetriou, M.; Nabi, I. R.; Coppolino, M.; Dedhar, S.; Dennis, J. W. Reduced contact-inhibition and substratum adhesion in epithelial cells expressing GlcNAc-transferase V. *J. Cell Biol.* **1995**, *130* (2), 383–392.

(45) Theocharis, A. D.; Tsara, M. E.; Papageorgacopoulou, N.; Karavias, D. D.; Theocharis, D. A. Pancreatic carcinoma is characterized by elevated content of hyaluronan and chondroitin sulfate with altered disaccharide composition. *Biochim. Biophys. Acta* **2000**, *1502* (2), 201–206.

(46) Theocharis, A. D.; Vynios, D. H.; Papageorgakopoulou, N.; Skandalis, S. S.; Theocharis, D. A. Altered content composition and structure of glycosaminoglycans and proteoglycans in gastric carcinoma. *Int. J. Biochem. Cell Biol.* **2003**, *35* (3), 376–390.

(47) Tsara, M. E.; Papageorgacopoulou, N.; Karavias, D. D.; Theocharis, D. A. Distribution and changes of glycosaminoglycans in neoplasias of rectum. *Anticancer Res.* **1995**, *15* (5B), 2107–2112.

(48) Iida, J.; Wilhelmson, K. L.; Ng, J.; Lee, P.; Morrison, C.; Tam, E.; Overall, C. M.; McCarthy, J. B. Cell surface chondroitin sulfate glycosaminoglycan in melanoma: role in the activation of pro-MMP-2 (pro-gelatinase A). *Biochem. J.* **2007**, *403* (3), 553–563.

(49) Price, M. A.; Colvin Wanshura, L. E.; Yang, J.; Carlson, J.; Xiang, B.; Li, G.; Ferrone, S.; Dudek, A. Z.; Turley, E. A.; McCarthy, J. B. CSPG4, a potential therapeutic target, facilitates malignant progression of melanoma. *Pigm. Cell Melanoma Res.* **2011**, *24* (6), 1148–1157.

(50) Bhavanandan, V. P. Glycosaminoglycans of cultured human fetal uveal melanocytes and comparison with those produced by cultured human melanoma cells. *Biochemistry* **1981**, *20* (19), 5595–5602.

(51) Stallcup, W. B.; Dahlin-Huppe, K. Chondroitin sulfate and cytoplasmic domain-dependent membrane targeting of the NG2 proteoglycan promotes retraction fiber formation and cell polarization. *J. Cell. Sci.* **2001**, *114* (Pt 12), 2315–2325.

(52) Chekenya, M.; Krakstad, C.; Svendsen, A.; Netland, I. A.; Staalesen, V.; Tysnes, B. B.; Selheim, F.; Wang, J.; Sakariassen, P. O.; Sandal, T.; Lonning, P. E.; Flatmark, T.; Enger, P. O.; Bjerkvig, R.; Sioud, M.; Stallcup, W. B. The progenitor cell marker NG2/MPG promotes chemoresistance by activation of integrin-dependent PI3K/Akt signaling. *Oncogene* **2008**, *27* (39), 5182–5194.

(53) Yang, J.; Price, M. A.; Li, G. Y.; Bar-Eli, M.; Salgia, R.; Jagedeeswaran, R.; Carlson, J. H.; Ferrone, S.; Turley, E. A.; McCarthy, J. B. Melanoma proteoglycan modifies gene expression to stimulate tumor cell motility, growth, and epithelial-to-mesenchymal transition. *Cancer Res.* **2009**, *69* (19), 7538–7547.

OPEN ACCESS Freely available online

PLOS ONE

Tightly Regulated and Homogeneous Transgene Expression in Human Adipose-Derived Mesenchymal Stem Cells by Lentivirus with Tet-Off System

Hiroyuki Moriyama[1*☯], Mariko Moriyama[1,2☯], Kei Sawaragi[1], Hanayuki Okura[2], Akihiro Ichinose[3], Akifumi Matsuyama[2], Takao Hayakawa[1]

1 Pharmaceutical Research and Technology Institute, Kinki University, Higashi-Osaka, Osaka, Japan, **2** Platform for Realization of Regenerative Medicine, Foundation for Biomedical Research and Innovation, Chuo-ku, Kobe, Hyogo, Japan, **3** Department of Plastic Surgery, Kobe University Hospital, Chuo-ku, Kobe, Hyogo, Japan

Abstract

Genetic modification of human adipose tissue–derived multilineage progenitor cells (hADMPCs) is highly valuable for their exploitation in therapeutic applications. Here, we have developed a novel single tet-off lentiviral vector platform. This vector combines (1) a modified tetracycline (tet)-response element composite promoter, (2) a multi-cistronic strategy to express an improved version of the tet-controlled transactivator and the blasticidin resistance gene under the control of a ubiquitous promoter, and (3) acceptor sites for easy recombination cloning of the gene of interest. In the present study, we used the cytomegalovirus (CMV) or the elongation factor 1 α (EF-1α) promoter as the ubiquitous promoter, and EGFP was introduced as the gene of interest. hADMPCs transduced with a lentiviral vector carrying either the CMV promoter or the EF-1α promoter were effectively selected by blasticidin without affecting their stem cell properties, and EGFP expression was strictly regulated by doxycycline (Dox) treatment in these cells. However, the single tet-off lentiviral vector carrying the EF-1α promoter provided more homogenous expression of EGFP in hADMPCs. Intriguingly, differentiated cells from these Dox-responsive cell lines constitutively expressed EGFP only in the absence of Dox. This single tet-off lentiviral vector thus provides an important tool for applied research on hADMPCs.

Citation: Moriyama H, Moriyama M, Sawaragi K, Okura H, Ichinose A, et al. (2013) Tightly Regulated and Homogeneous Transgene Expression in Human Adipose-Derived Mesenchymal Stem Cells by Lentivirus with Tet-Off System. PLoS ONE 8(6): e66274. doi:10.1371/journal.pone.0066274

Editor: Niels Olsen Saraiva Câmara, Universidade de Sao Paulo, Brazil

Received December 20, 2012; **Accepted** May 2, 2013; **Published** June 12, 2013

Funding: This work was supported in part by MEXT KAKENHI Grant Number 23791304 to M.M. and 24791927 to H.M. This work was also supported in part by grants from the Ministry of Health, Labor, and Welfare of Japan and a grant from the Program for Promotion of Fundamental Studies in Health Sciences of the National Institute of Biomedical Innovation (NIBIO). The funders had no role in study design, data collection and analysis, decision to publish, or preparation of the manuscript.

Competing Interests: The authors have declared that no competing interests exist.

* E-mail: moriyama@phar.kindai.ac.jp

☯ These authors contributed equally to this work.

Introduction

Human adipose tissue–derived mesenchymal stem cells (MSCs), also referred to as human adipose tissue–derived multilineage progenitor cells (hADMPCs), are multipotent stem cells that can differentiate into various types of cells, including hepatocytes [1], cardiomyoblasts [2], pancreatic cells [3], and neuronal cells [4–6]. They can be easily and safely obtained from lipoaspirates without posing serious ethical issues and can also be expanded ex vivo under appropriate culture conditions. Moreover, MSCs, including hADMPCs, have the ability to migrate to injured areas and secrete a wide variety of cytokines and growth factors necessary for tissue regeneration [7–11]. Because of their hypoimmunogenicity and immune modulatory effects, hADMPCs are good candidates for gene delivery vehicles for therapeutic purposes [12]. Thus, hADMPCs are an attractive material for cell therapy and tissue engineering, making the development of technologies for permanent and highly controlled genetic modification of hADMPCs quite valuable.

Lentiviral vectors are powerful tools for gene transfer in primary human cells, as they integrate into the host cell genome, resulting in stable long-term transgene expression. Lentiviral vectors are less prone to transcriptional silencing than oncoretroviral vectors [13,14]; however, researchers have reported that transgene silencing occurs when a strong promoter, such as the cytomegalovirus (CMV) promoter, is used in certain cell types, especially embryonic stem cells [15–17]. Recently, it has been reported that the CMV promoter is also silenced in rat bone marrow–derived MSCs [18,19], suggesting that consideration of promoter used in the lentiviral vector is one of the most critical issues.

In addition to the choice of promoters, the specific gene expression system can have a great impact on the properties and functions of the infected hADMPCs. In order to express therapeutic genes, master regulatory genes, or microRNAs, the development of a tightly regulated, inducible gene expression system is required. The tetracycline (tet)-regulated transgene expression (tet-off) system is the most advanced system being used in gene therapy trials [20]. Two expression cassettes need to be delivered for use of the tet-off system: the regulatory unit for the constitutive expression of the transactivator (tTA), and the tet-controlled responsive unit for the expression of the gene of interest. Traditionally, these 2 cassettes should be transduced separately to establish tet-inducible cell lines. This time-consuming process